NASA TECHNICAL NOTE

NASA TN D-3268

NASA TN D-3268

EXPERIMENTAL INVESTIGATION OF PARAMETERS AND MATERIALS FOR FRAGMENTING-TUBE ENERGY-ABSORPTION PROCESS

by John R. McGehee

Langley Research Center
Langley Station, Hampton, Va.

NATIONAL AERONAUTICS AND SPACE ADMINISTRATION • WASHINGTON, D. C. • FEBRUARY 1966

NASA TN D-3268

EXPERIMENTAL INVESTIGATION OF PARAMETERS AND MATERIALS FOR FRAGMENTING-TUBE ENERGY-ABSORPTION PROCESS

By John R. McGehee

Langley Research Center
Langley Station, Hampton, Va.

NATIONAL AERONAUTICS AND SPACE ADMINISTRATION

For sale by the Clearinghouse for Federal Scientific and Technical Information
Springfield, Virginia 22151 – Price $2.00

EXPERIMENTAL INVESTIGATION OF PARAMETERS AND MATERIALS FOR FRAGMENTING-TUBE ENERGY-ABSORPTION PROCESS

By John R. McGehee
Langley Research Center

SUMMARY

An experimental investigation has been conducted to determine the variation of the average fragmenting stress of 2024-T3 aluminum-alloy tubing with the pertinent parameters of the process. The investigation was conducted for a range of tube-wall-thickness—die-forming-radius ratios from 0.172 to 0.614, a range of tube-inside-diameter—die-forming-radius ratios from 1.706 to 10.400, and a rate of displacement of approximately 1 in./min (0.4 mm/s). A brief experimental investigation was performed to demonstrate the use of tubes of 7075-T6 aluminum alloy, AZ31B magnesium alloy, and chrome-molybdenum steel (AISI 4130) in a cold-water-quenched condition in the fragmenting process.

The results of this investigation indicate that the average fragmenting stress of 2024-T3 aluminum-alloy tubing varies directly as the cube root of the tube-inside-diameter—die-forming-radius ratio and inversely as a function of the tube-wall-thickness—die-forming-radius ratio. The average fragmenting stress for 2024-T3 aluminum-alloy tubing computed from a derived empirical equation is in fair agreement with the experimental data for the range of parameters investigated. The maximum value of the average fragmenting stress may be obtained when the magnitude of the stress fluctuations about the average value is a minimum and when the largest values of tube-wall-thickness—die-forming-radius ratio and tube-inside-diameter—die-forming-radius ratio are employed. The fragmenting of tubes of 2024-T3 aluminum alloy, 7075-T6 aluminum alloy, AZ31B magnesium alloy, and chrome-molybdenum steel (AISI 4130) in a cold-water-quenched condition has been demonstrated. The results of the brief materials investigation indicate that the energy-absorption capability of the fragmenting of tubes of various materials generally increases with increasing material yield stress. The AISI 4130 steel was the most efficient tubing on the basis of energy-absorption capability per pound force (N) of material.

INTRODUCTION

Energy-absorption processes possessing high energy-absorption capability have received considerable attention in recent years as a result of requirements established in connection with spacecraft landing systems. The most promising energy-absorption systems, those with very high energy-absorption capability, appear to be systems which combine material deformation and friction (ref. 1). Some of the more efficient energy-absorption processes that have been recently investigated are reported in references 1, 2, and 3. A preliminary experimental investigation of a highly efficient energy-absorption process, the fragmenting-tube process, was reported in reference 4.

In the fragmenting-tube process, energy is absorbed through the force developed when a frangible tube is pressed over a die. The die is shaped so that the portion of the tube in contact with the die is split into segments and the segments are broken into small fragments. A fluctuating force is developed by the fragmenting process, but the force about which the fluctuation occurs is approximately constant. The breaking and dispersing of the segments of the tube permit, with proper design, the entire length of the tube to be employed as the working stroke. It was tentatively established in reference 4 that the principal parameters of the fragmenting-tube process are the tube-wall-thickness—die-forming-radius ratio, the mechanical properties of the tubing material, and the rate of displacement of the tubing over the die. Limited experimental data were presented and the use of the process in a load-alleviation application was demonstrated.

The present investigation was conducted to establish the average fragmenting stress (average column load divided by cross-sectional area of the tube) obtained from 2024-T3 aluminum-alloy tubing employed in the fragmenting-tube energy-absorption process and to extend relative to the data of reference 4, the ranges of tube wall thicknesses and diameters investigated. The data were obtained for tube wall thicknesses from 0.057 to 0.430 in. (0.145 to 1.092 cm), tube outside diameters from 0.861 to 3.967 in. (2.187 to 10.076 cm), die forming radii from 0.125 to 0.758 in. (0.317 to 1.925 cm), and a rate of displacement of approximately 1 in./min (0.4 mm/s). The use of other alloys and materials in this process was demonstrated by fragmenting tubes of 7075-T6 aluminum alloy, AZ31B magnesium alloy, and chrome-molybdenum steel (AISI 4130) in a cold-water-quenched condition.

SYMBOLS

The units used for the physical quantities in this paper are given both in the U.S. Customary Units and in the International System of Units (SI). Factors relating the two

systems are given in reference 5 and those used in the present investigation are presented in appendix A.

A	area of cross section of tubing, $\pi(D_o - t)t$, in^2 (cm^2)
d	tube axial displacement, in. (cm)
D	diameter, in. (cm)
F	axial force, lbf (N)
G	functional notation
K	constant
l	length, in. (cm)
r	forming radius of die, in. (cm)
t	wall thickness of tubing, in. (cm)
σ	stress, F/A, psi (N/m^2)

Subscripts:

av	average
f	fragmenting
i	inside
max	maximum
min	minimum
o	outside
s	die shaft
y	yield

APPARATUS

Testing Machine and Instrumentation

This investigation was conducted in the 1.2 megapound-capacity (5.3-MN) universal static hydraulic testing machine at the Langley Research Center. The load range of this machine was more than that required for this investigation, but the structural rigidity of the machine reduced the possibility of elastic deformation of the machine affecting measured test forces. The test setup, as shown in figure 1, was the same as that used in reference 4 for the investigation conducted at low rates of displacement.

The outputs from strain gages on a thin cantilever beam activated by the weighing system of the testing machine and from a linear potentiometer were recorded simultaneously on a two-channel pen recorder. The response time for full-scale deflection of the pens, 10 in. (25.4 cm), was 1 second.

Dies

The forming section of the dies was semicircular in cross section and circular in planform. The dies were machined from a mild steel and were case hardened to a depth of approximately 0.06 in. (0.15 cm). A sketch of the die configuration and the pertinent dimensions of the dies are shown in table I. The procedure employed for determining the radii of the forming section of the dies is described in appendix B.

TEST PROCEDURE

The test procedures and pertinent information concerning preparation of tube specimens for the short-tube compression tests, the materials investigation, and the parametric investigation are presented. The accuracy of the pertinent dimensions of the tube specimens, dies, and recording instrumentation is given.

The fragmenting regime, which was defined in reference 4, includes the range of parameters within which the segments of the tube are broken before the leading edges of the segments leave the forming section of the die. A sketch illustrating the process is shown in figure 2. The fragmenting-tube specimens were restricted in length by maintaining initial length-diameter ratios of 10 or less (short-column range) to reduce the possibility of column buckling. The inner surface of the tube specimens and the working surface of the dies were coated with a mixture of light oil and molybdenum disulphide powder to reduce friction in order to obtain repeatable results.

Short-Tube Compression Tests

The yield stress is one of the primary material mechanical properties of importance in the fragmenting-tube process, because the material yield stress is an upper limit for the average fragmenting stress. The yield stresses of the materials investigated were determined from short-tube compression tests. The short-tube specimens were cut from unfragmented sections of tubes which had previously been fragmented. In an effort to obtain consistent results, a length-thickness ratio of 10 was used.

Fragmenting-Tube Tests

Parametric investigation.- The results of the experimental investigation of reference 4 indicate that the fragmenting force or stress is very sensitive to changes in t/r

and independent of the variation of t/D_o for the ranges of these parameters investigated. On the basis of these results, the program for the present investigation was formulated to isolate the principal parameters and thus permit evaluation of their effects with a minimum of interaction. Since the fragmenting stress is primarily affected by changes in t/r, it was necessary to determine tube wall thicknesses to closer tolerances than those specified by the tubing manufacturer. To eliminate the effects of slight differences in die contours, the program was planned so that the ratio t/r could be varied over the desired range by testing specimens of different wall thicknesses on the same die. However, the use of different dies for defining the variation of the fragmenting stress with t/D_o was necessary. This portion of the investigation was conducted by using 2024-T3 aluminum-alloy tubing. (See table II for specimen dimensions.) To obtain the desired tube wall thicknesses within planned tolerances, oversized tubing was machined to the desired thicknesses. Prior to machining, the tubing was cut into the desired lengths and forced onto steel mandrels having diameters approximately 0.5 percent greater than the inside diameter of the tubing. The oversized steel mandrel was used in an effort to obtain uniform tube wall thickness throughout the length of the specimen. With the tube on the mandrel, material was machined from the outside of the tube until the desired wall thickness was obtained. The specimens were machined from as-purchased tubing having the following dimensions:

D_o		t	
in.	cm	in.	cm
1	2.54	0.21	0.53
2	5.08	.35	.89
4	10.16	.44	1.12

To reduce the magnitude of the force required to start the fragmenting process, all specimens tested in this phase of the investigation were machined with a 14° outside taper (see fig. 2) on the wall thickness at the die end of the specimens.

Tests were conducted on tube specimens having a range of wall thicknesses from 0.057 to 0.430 in. (0.145 to 1.092 cm) and a range of outside diameters from 0.861 to 3.967 in. (2.187 to 10.076 cm). The ranges of the principal parameters investigated were as follows:

t/r ..... 0.172 to 0.614
t/D_o ..... 0.040 to 0.205
D_i/r ..... 1.706 to 10.400
σ_y ..... 42 ksi (290 MN/m^2)

Materials investigation.- The materials investigation was conducted by testing specimens of 2024-T3 aluminum alloy, 7075-T6 aluminum alloy, AZ31B magnesium alloy, and chrome-molybdenum steel (AISI 4130). These tests were made to demonstrate the use of various alloys and materials in the fragmenting-tube process; consequently, only a brief test program was conducted. The steel specimens were tested in each of the following heat-treated conditions: annealed, drawn at 350° F (450° K), drawn at 500°F (533° K), quenched in oil, and quenched in cold water. Specimens of 7075-T6 aluminum alloy, AZ31B magnesium alloy, and chrome-molybdenum steel (AISI 4130) had a wall thickness of 0.065 in. (0.165 cm) and an outside diameter of 1.000 in. (2.540 cm). A 7° outside taper was machined on the wall thickness at the die end of the specimens to reduce the magnitude of the force required to start the fragmenting process.

The ranges of the principal parameters for these three materials were as follows:

t/r	0.333 to 0.644
t/D_o	0.065
D_i/r	4.461 to 8.614
σ_y	16 to 210 ksi (110 to 1448 MN/m^2)

The ranges of the parameters for the 2024-T3 aluminum-alloy specimens are given in the preceding section.

Accuracy of Measurements

The accuracy of the pertinent measurements was determined to be as follows:

t, in. (cm)	±0.001 (±0.003)
D, in. (cm)	±0.001 (±0.003)
l, in. (cm)	±0.001 (±0.003)
r, in. (cm)	±0.001 (±0.003)
d, in. (cm)	±0.05 (±0.13)
F, lbf (N)	±0.5 percent of indicated force or ±0.1 percent of dial capacity

RESULTS AND DISCUSSION

The results of the short-tube compression tests, the fragmenting-tube parametric investigation, and the fragmenting-tube materials investigation are presented and an empirical equation for the average fragmenting stress as a function of the pertinent parameters is derived. The data obtained during this experimental investigation are presented in table II.

Short-Tube Compression Tests

The force-displacement data obtained from compression tests of several short-tube specimens of each material employed in this investigation were used to define the material yield stress. These data for 2024-T3 aluminum alloy, 7075-T6 aluminum alloy, AZ31B magnesium alloy, and AISI 4130 steel in a cold-water-quenched condition are compared with minimum values of tensile yield strength quoted from reference 6:

Material	Average test value	Handbook value
2024-T3 aluminum alloy	42 ksi $\left(290\ MN/m^2\right)$	42 ksi $\left(290\ MN/m^2\right)$
7075-T6 aluminum alloy	74 ksi $\left(510\ MN/m^2\right)$	73 ksi $\left(503\ MN/m^2\right)$
AZ31B magnesium alloy	17 ksi $\left(117\ MN/m^2\right)$	16 ksi $\left(110\ MN/m^2\right)$
AISI 4130 steel, cold-water-quenched condition	210 ksi $\left(1448\ MN/m^2\right)$	----------

Parametric Investigation

Fragmenting-tube tests.- The data obtained in the preliminary experimental investigation of reference 4 were analyzed by assuming that one of the primary dimensionless parameters was tube-wall-thickness—tube-outside-diameter ratio t/D_o. However, during the analysis of the data obtained in the present investigation, the use of tube-inside-diameter—die-forming-radius ratio D_i/r as a controlling parameter appeared to define the variation of the experimental data for the extended range of t/D_o more closely. The data presented in this paper are analyzed by using D_i/r instead of t/D_o as one of the principal dimensionless parameters.

Typical axial-force variations as a function of axial displacement are shown in figure 3 for a constant value of t/r and for several values of D_i/r. The 14^o outside taper on the tube wall thickness was not sufficient, in some cases, to eliminate the large force required to initiate fragmenting (see fig. 3(a)). However, it was shown in reference 4 that a more gradual ($\approx 7^o$) outside taper was sufficient to eliminate the force peak associated with the initiation of fragmenting on an unaltered tube. The maximum, average, and minimum fragmenting forces are defined as shown for the typical force-displacement data presented in this figure. The average fragmenting force shown for each of the curves was determined by dividing the area under the curves, obtained with a planimeter, by the corresponding displacement.

The largest value of average fragmenting stress that may be obtained is a function of, in addition to the controlling parameters of the process, the magnitude of the stress or force fluctuations about the average value. The force peaks associated with the

initiation of fragmenting being neglected, the maximum and minimum values of fragmenting force as percentages of the average fragmenting force are shown in figure 4 as a function of t/r for three values of D_i/r. Once fragmentation has been initiated the fragments occur randomly and the magnitude of the force fluctuations depends upon the portion of the tube circumference being deformed. The data shown in figure 4 are for the maximum and minimum forces (see fig. 3) occurring during the testing of each of the tube specimens, and scatter is to be expected. However, the trends indicated by the data show that the magnitude of the force fluctuations is reduced at the lower values of t/r. This trend would be expected for t/r values of approximately 0.25 or less because the tube segments roll and do not fragment. Consequently, an essentially constant force or stress results, with the magnitude varying with the roll radius. For values of t/r above 0.5, the trends indicated by the data once again show a reduction in the magnitude of the force fluctuations. This reduction may be attributed to the smaller lengths of fragments which result at higher values of t/r. At the larger values of t/r, the meridional splits (which produce the segments) terminate very near the beginning of the curvature of the die forming section and, as a result, the fragment-producing fracture occurs within the forming section of the die. Thus the base of the tube remains highly loaded as individual segments fragment.

The variations of the maximum and minimum fragmenting forces with D_i/r are shown in figure 5 for a constant value of t/r of 0.460. The magnitude of the stress fluctuations decreases with increasing D_i/r for the range of D_i/r investigated. To simplify the explanation of this result, the D_i/r ratio at a constant value of t/r may be converted to a D_i/t ratio as follows:

$$\frac{D_i}{r} = K\frac{D_i}{t}$$

where $K = t/r$. Observations made during the conduct of the experimental program revealed that the number of circumferential segments formed increased as D_i/t was increased. With many circumferential segments, the fragmenting of any single segment would have less effect on the load supported by the tubular column than would be the case for a single segment fragmenting when there were few segments. This trend indicates that a more efficient operation may result at larger values of D_i/r.

Empirical relation for fragmenting stress.- The experimental data are presented in figures 6 and 7 as plots of the average fragmenting stress as a function of D_i/r and t/r, respectively. As shown in figure 6 the average fragmenting stress for a constant t/r increases as D_i/r increases. This effect may be attributed to a greater percentage of material being worked to failure, since it has been observed that a greater number of circumferential splits are formed when the tube diameter is increased relative to the die

radius at a constant t/r. The data in figure 7 show that the average fragmenting stress at a constant D_i/r increases with increasing values of t/r. It has been observed that increases in t/r, for a constant D_i/r, result in the production of smaller fragments. As a result, more of the material is worked to failure as t/r is increased and a greater average fragmenting stress is obtained.

In examining the results of figure 7, it appears that the curves have the same form as a portion of a rectangular hyperbola rotated through 45° and translated along the t/r axis. Since a reciprocal relationship exists between the ordinate and abscissa for such a hyperbola, the reciprocal of the average fragmenting stress was plotted against t/r for given values of D_i/r (see fig. 8). Linear fairings of these data intersected the t/r axis at a value of 0.7. The equation for the reciprocal of the average fragmenting stress is then

$$\frac{1}{\sigma_{f,av}} = (0.7 - t/r)K \tag{1}$$

where K is the slope of the fairing for a constant value of D_i/r. Equation (1) may be rewritten as

$$\sigma_{f,av}(0.7 - t/r) = G\left(D_i/r\right) \tag{2}$$

By using equation (2), data from the faired curves of figures 6 and 7 are plotted in figure 9 as the product of σ_f and $(0.7 - t/r)$ against D_i/r. Values of t/r varied from 0.300 to 0.600. The data are plotted on logarithmic scales to simplify the determination of the D_i/r function. The data are faired linearly and the equation defining the curve is

$$\sigma_{f,av}(0.7 - t/r) = 1.90\sqrt[3]{D_i/r} \tag{3}$$

The empirical equation for the average fragmenting stress for 2024-T3 aluminum-alloy tubing is

$$\sigma_{f,av} = \frac{1.90\sqrt[3]{D_i/r}}{0.7 - t/r} \tag{4}$$

A comparison between the experimental average fragmenting stress and the average fragmenting stress computed from equation (4) is shown in figure 10. Average fragmenting stress is plotted as a function of t/r for several nominal values of D_i/r. The average fragmenting stress computed from the empirical equation is in fair agreement with the experimental data for the variation of $\sigma_{f,av}$ with t/r. It should be noted,

however, that for a t/r of 0.6, at the lower values of D_i/r, only scanty experimental data were obtained and the agreement between experimental and computed data is not as good. The deviation of the mean values of the experimental data from the calculated values for the specific D_i/r ratios may be attributed to slight differences in die contours since, as a result of the test program, the data for each nominal value of D_i/r were obtained from a different die.

The average fragmenting stress as a function of the principal parameters for 2024-T3 aluminum-alloy tubing is presented in a form more useful to the designer in figure 10(b). However, because of the variability of the tubing mechanical properties, a proof test of a particular design should be performed prior to incorporation in an operating system.

Material Investigation

Fragmenting-tube tests.- Typical axial-force variations with displacement are shown in figure 11 for tubes of 7075-T6 aluminum alloy, AZ31B magnesium alloy, and chrome-molybdenum steel (AISI 4130) in a cold-water-quenched condition. Similar data for 2024-T3 aluminum tubes are shown in figure 3 for a value of t/r of 0.300. The data for the three materials shown in figure 11 were obtained by fragmenting the tubes at a value of t/r of 0.396.

The chrome-molybdenum steel (AISI 4130) specimens in the annealed, 350° F (450° K) drawn, and the 500° F (533° K) drawn conditions split and rolled or failed due to column buckling for the range of t/r used in this investigation. The oil-quenched specimens were fragmented successfully only at the largest value of t/r, 0.644. The cold-water-quenched AISI 4130 steel, the 7075-T6 aluminum alloy, and the AZ31B magnesium specimens fragmented satisfactorily over the test range of t/r.

The fragmenting process results in working the tube material through the yield stress into the plastic range until the material reaches the fracture stress where fragmenting occurs. Therefore it was expected that the average fragmenting stress would increase for the fragmenting of tubes of materials with increased values of yield stress. The variation of the average fragmenting stress with t/r for the materials tested in this investigation is shown in figure 12 for a range of D_i/r of 4.461 to 8.614. The data in this figure for AZ31B magnesium alloy, 7075-T6 aluminum alloy, and AISI 4130 steel indicate that the average fragmenting stress does increase for materials possessing increased values of yield stress. However, when the data for the 2024-T3 aluminum alloy $\left(\sigma_y = 42 \text{ ksi } (290 \text{ MN/m}^2)\right)$ and the 7075-T6 aluminum alloy $\left(\sigma_y = 74 \text{ ksi } (510 \text{ MN/m}^2)\right)$ are compared, it is obvious that there are other mechanical properties which offset the increase in fragmenting stress due to the increased yield stress. It is generally known that the 7075-T6 aluminum alloy is more crack sensitive than the 2024-T3 aluminum alloy

and, during the tests, it appeared that the circumferential segments of the 7075-T6 aluminum alloy fragmented with a smaller penetration into the die than did those of the 2024-T3 aluminum alloy. As a result, the average fragmenting stress developed by the 7075-T6 was smaller than would have been expected when considering the higher yield stress of this material relative to the 2024-T3 material. However, it is of interest to note that the 7075-T6 alloy fragmented at a larger value of t/r than did the 2024-T3 alloy.

The mechanical properties required of a material for use in this process have not been implicitly defined. However, it appears that the minimum value of the ratio of bend radius to sheet thickness for a material with a 90° cold bend represents a value of t/r below which fragmenting will not occur. For example, reference 7 gives an average value of minimum bend radius of 4 sheet thicknesses for a 90° cold bend of a 0.06-inch-thick (0.15-cm) 2024-T3 aluminum-alloy sheet material. This value of bend radius would correspond to a value of t/r of 0.25. All fragmenting tests conducted for values of t/r less than 0.25 with this material have resulted in a rolling phenomenon with no fragmenting occurring. The upper limit of the fragmenting range (maximum value of t/r at which fragmenting will occur) is a function of the tubular-column yield stress and the average fragmenting stress, since column failure will occur if the average fragmenting stress exceeds the column yield stress.

Energy-absorption capability for different materials.- The energy-absorption capabilities of various materials and processes are presented in bar graph form in figure 13. The energy-absorption capability of each material is expressed as the ratio of the maximum energy obtained from the various tubing materials per unit mass of material, and those values shown for the fragmenting-tube process do not include the weight of the die. The energy-absorption capability from the crushing of 4-mil (0.1-mm) 5052 aluminum honeycomb with 0.25-in. (6-mm) hexagonal cell structure was obtained from reference 8. The energy-absorption capability of the crushing of 7075-T6 cellular aluminum alloy (cell structures, 35 mesh, crushed to 70 percent of initial length, length-diameter ratio of 1.28) was obtained from reference 9. The energy-absorption capabilities shown for the fragmenting of tubes of AZ31B magnesium alloy, 2024-T3 aluminum alloy, 7075-T6 aluminum alloy, and AISI 4130 steel in a cold-water-quenched condition were based on data obtained for each of these materials at the maximum value of t/r and for a value of D_i/r of approximately 8.6. The data shown in the bar graph illustrate the increased energy-absorption capability of materials employed in the fragmenting-tube process as compared with processes involving crushing of the material. The data also indicate that for materials employed in the fragmenting-tube process, energy-absorption capability increases with increasing material yield stress. The fragmenting of AISI 4130 steel tubing was found to be the most efficient on the basis of energy absorption per unit mass of material. The fragmenting of 7075-T6 aluminum-alloy tubing and AISI 4130 steel

tubing could result in greater energy-absorption capability than that shown in the bar graph, since it appears that these materials would fragment at larger values of t/r than were investigated. For example, AISI 4130 steel in a cold-water-quenched condition would have, assuming that it was fragmented to obtain an average fragmenting stress of 90 percent of the yield stress (a condition which has been achieved by using 2024-T3 aluminum-alloy tubing), an energy-absorption capability of 55 600 ft-lbf/lbf (16 900 J/N).

CONCLUDING REMARKS

The results of the experimental investigation of the fragmenting-tube energy-absorption process show that the average fragmenting stress of 2024-T3 aluminum-alloy tubing varies directly as the cube root of the tube-inside-diameter—die-forming-radius ratio and inversely as a function of tube-wall-thickness—die-forming-radius ratio. An empirical equation has been derived to define the variation of the average fragmenting stress of 2024-T3 aluminum-alloy tubing with the pertinent parameters. The average fragmenting stress computed from the empirical equation was in fair agreement with the experimental data.

The mechanical properties required of a material for use in this process have not been implicitly defined. However, it appears that the minimum value of the ratio of bend radius to sheet thickness for a material with a 90° cold bend represents a value of tube-wall-thickness—die-forming-radius ratio below which fragmenting will not occur. The upper limit of the fragmenting range (maximum value of tube-wall-thickness—die-forming-radius ratio at which fragmenting will occur) is a function of the tubular-column yield stress and the average fragmenting stress, since column failure will occur if the average fragmenting stress exceeds the column yield stress.

The fragmenting phenomenon produces a fluctuating stress which varies with displacement, but, for a fixed set of parameters, the stress about which the fluctuation occurs is approximately constant. The maximum value of the average fragmenting stress may be developed at large values of tube-wall-thickness—die-forming-radius ratio and tube-inside-diameter—die-forming-radius ratio when the magnitude of the stress fluctuations is a minimum. The results indicate that the magnitude of the fluctuations is a maximum at a tube-wall-thickness—die-forming-radius ratio of approximately 0.5 and decreases for values of this parameter less than or greater than 0.5. The magnitude of the stress fluctuations decreases with increasing tube-inside-diameter—die-forming-radius ratio for the range of this parameter investigated.

The fragmenting of tubes of 2024-T3 aluminum alloy, 7075-T6 aluminum alloy, AZ31B magnesium alloy, and chrome-molybdenum steel (AISI 4130) in a cold-water-quenched condition has been demonstrated. The energy-absorption capability of tubes of various materials generally increases with increasing material yield stress. The fragmenting of AISI 4130 steel tubing was found to be the most efficient on the basis of energy absorption per unit mass of material. The efficiency of the fragmenting-tube process for aluminum-alloy and steel tubing is substantially greater than for the crushing of aluminum-alloy honeycomb and cellular construction.

Langley Research Center,
National Aeronautics and Space Administration,
Langley Station, Hampton, Va., September 14, 1965.

APPENDIX A

CONVERSION OF U.S. CUSTOMARY UNITS TO SI UNITS

The International System of Units (SI) was adopted by the Eleventh General Conference on Weights and Measures, Paris, October 1960, in Resolution No. 12 (ref. 5). Conversion factors for the units used herein are given in the following table:

Physical quantity	U.S. Customary Unit	Conversion factor (*)	SI unit
Energy per unit weight	ft-lbf/lbf	0.3048	joules/newton (J/N)
Force	lbf	4.448	newtons (N)
	kips	4.448×10^3	newtons (N)
Length	in.	0.0254	meters (m)
	micron	1.00×10^{-6}	meters (m)
Stress	psi = lbf/in^2	6.895×10^{-3}	newton/meter^2 (N/m^2)
Temperature . . .	^oF	(5/9) (^oF + 459.67)	degrees Kelvin (^oK)

*Multiply value given in U.S. Customary Unit by conversion factor to obtain equivalent value in SI unit.

Prefixes to indicate multiples of units are as follows:

Prefix	Multiple
mega (M)	10^6
kilo (k)	10^3
centi (c)	10^{-2}
milli (m)	10^{-3}
micro (μ)	10^{-6}

APPENDIX B

PROCEDURE FOR MEASURING RADII OF DIE FORMING SECTION

The magnitude of the average fragmenting force obtained from a tube-die combination is extremely sensitive to the shape and radius of the forming section of the die. The procedure used to define the shape and the radii of the forming section of the various dies to an accuracy of 0.001 in. (0.003 cm) is described. A full mold of the die forming section was cast using a low melting point alloy having the constituents in the percentages as shown:

Bismuth	50.0%
Tin	13.3%
Lead	26.7%
Cadmium	10.0%

This alloy expands slightly during a 24-hour period following casting. Therefore, the die molds were poured and allowed to remain in the dies for 24 hours. The castings were then removed from the dies and sectioned along radial lines. To obtain a sharp definition of the edge of the casting, the sections were mounted in plastic and polished. The plastic-embedded sections were mounted in a microscope and the coordinates of several points on the semicircular portion of the sections were obtained. The microscope table can be traversed along two axes and the coordinates of the points can be read consistently to ±5 microns (5μ). The coordinates of a set of two points, measured from a point on the circular portion of the die, were substituted into the following equation to determine the radius of the die forming section:

$$r = \frac{1}{2}\left[\frac{\left(x_2^2 + y_2^2\right)y_1 - \left(x_1^2 + y_1^2\right)y_2}{x_1y_2 - x_2y_1} + \frac{\left(x_2^2 + y_2^2\right)x_1 - \left(x_1^2 + y_1^2\right)x_2}{x_2y_1 - x_1y_2}\right]^{1/2}$$

Several values of the radius, for different portions of the section, were obtained. The average of these values was used in the analysis of the experimental data.

REFERENCES

1. Esgar, Jack B.: Survey of Energy-Absorption Devices for Soft Landing of Space Vehicles. NASA TN D-1308, 1962.

2. Kroell, C. K.: A Simple, Efficient, One Shot Energy Absorber. Shock, Vib. and Assoc. Environments, Bull. 30, Pt. III, U.S. Dept. Defense, Feb. 1962, pp. 331-338.

3. Meyers, W. M.; and Lorsch, H. G.: RF Transparent, Energy Absorbing, Structural Elements – Phase I. NASA CR-53479, 1964.

4. McGehee, John R.: A Preliminary Experimental Investigation of an Energy-Absorption Process Employing Frangible Metal Tubing. NASA TN D-1477, 1962.

5. Mechtly, E. A.: The International System of Units – Physical Constants and Conversion Factors. NASA SP-7012, 1964.

6. Anon.: Metallic Materials and Elements for Flight Vehicles Structures. MIL-HDBK-5, U.S. Dept. Defense, Aug. 1962. (Supersedes MIL-HDBK-5, 1961.)

7. Anon.: Alcoa Aluminum Handbook. Aluminum Co. of Am., c.1962.

8. Daigle, D. L.; and Lonborg, J. O.: Evaluation of Certain Crushable Materials. Tech. Rept. No. 32-120 (Contract No. NASw-6), Jet Propulsion Lab., C.I.T., Jan. 13, 1961.

9. Lipson, S.: Cellular Aluminum for Use in Energy Dissipation Systems. NASA CR-93, 1964.

TABLE I.- DIMENSIONS OF DIES

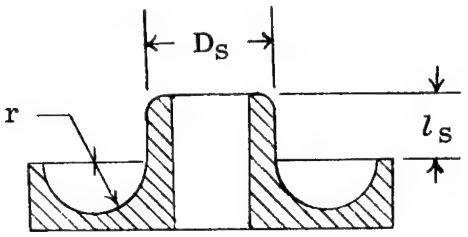

r		D_S		l_S	
in.	cm	in.	cm	in.	cm
Materials investigation					
0.101	0.257	0.870	2.210	1.000	2.540
.115	.292	.870	2.210	1.000	2.540
.125	.318	.870	2.210	1.000	2.540
.132	.335	.870	2.210	1.000	2.540
.155	.394	.870	2.210	1.000	2.540
.158	.401	.870	2.210	1.000	2.540
.164	.417	.870	2.210	1.000	2.540
.195	.495	.870	2.210	1.000	2.540
Parametric investigation					
0.125	0.318	1.300	3.302	1.000	2.540
.249	.632	1.300	3.302	1.000	2.540
.344	.874	.624	1.585	1.000	2.540
.378	.960	1.300	3.302	1.000	2.540
.430	1.092	1.300	3.302	1.000	2.540
.506	1.285	1.300	3.302	1.000	2.540
.626	1.590	1.300	3.302	1.500	3.810
.630	1.600	1.300	3.302	1.000	2.540
.738	1.875	3.250	8.255	3.000	7.620
.758	1.925	1.300	3.302	1.000	2.540

TABLE II.- SPECIMEN DIMENSIONS AND TEST RESULTS

t		r		D_i		t/r	D_i/r	$F_{f,av}$		$\sigma_{f,av}$		Operating regime
in.	cm	in.	cm	in.	cm			kips	kN	psi	MN/m^2	
2024-T3 aluminum alloy												
0.103	0.262	0.344	0.874	0.588	1.494	0.299	1.709	1.40	6	6 260	43	Fragmented
.103	.262	.344	.874	.588	1.494	.299	1.709	1.46	6	6 520	45	Fragmented
.103	.262	.344	.874	.588	1.494	.299	1.709	1.36	6	6 080	42	Fragmented
.103	.262	.344	.874	.588	1.494	.299	1.709	1.38	6	6 160	42	Fragmented
.120	.305	.344	.874	.588	1.494	.349	1.709	1.84	8	6 900	48	Fragmented
.120	.305	.344	.874	.588	1.494	.349	1.709	1.81	8	6 780	47	Fragmented
.120	.305	.344	.874	.588	1.494	.349	1.709	1.90	8	7 120	49	Fragmented
.120	.305	.344	.874	.588	1.494	.349	1.709	1.92	9	7 190	50	Fragmented
.136	.345	.344	.874	.589	1.496	.395	1.712	2.88	13	9 300	64	Fragmented
.137	.348	.344	.874	.588	1.494	.398	1.709	2.40	11	7 700	53	Fragmented
.137	.348	.344	.874	.588	1.494	.398	1.709	2.57	11	8 240	57	Fragmented
.137	.348	.344	.874	.588	1.494	.398	1.709	2.65	12	8 500	59	Fragmented
.154	.391	.344	.874	.589	1.496	.448	1.712	3.77	17	10 500	72	Fragmented
.154	.391	.344	.874	.589	1.496	.448	1.712	3.30	15	9 200	63	Fragmented
.154	.391	.344	.874	.589	1.496	.448	1.712	3.46	15	9 600	66	Fragmented
.155	.394	.344	.874	.587	1.491	.451	1.706	3.50	16	9 700	67	Fragmented
.171	.434	.344	.874	.589	1.496	.497	1.712	4.66	21	11 400	79	Fragmented
.171	.434	.344	.874	.589	1.496	.497	1.712	5.40	24	13 200	91	Fragmented
.171	.434	.344	.874	.589	1.496	.497	1.712	4.65	21	11 400	79	Fragmented
.171	.434	.344	.874	.589	1.496	.497	1.712	5.60	25	13 700	94	Fragmented
.189	.480	.344	.874	.588	1.494	.549	1.709	7.28	32	15 800	109	Fragmented
.189	.480	.344	.874	.588	1.494	.549	1.709	7.00	31	15 200	105	Fragmented
.189	.480	.344	.874	.588	1.494	.549	1.709	8.12	36	17 620	121	Fragmented
.189	.480	.344	.874	.588	1.494	.549	1.709	8.63	38	18 700	129	Fragmented
.205	.521	.344	.874	.589	1.496	.596	1.712	12.53	56	24 460	169	Fragmented
.205	.521	.344	.874	.589	1.496	.596	1.712					Buckled
.205	.521	.344	.874	.589	1.496	.596	1.712					Buckled
.205	.521	.344	.874	.589	1.496	.596	1.712					Buckled
.205	.521	.344	.874	.589	1.496	.596	1.712					Buckled
.057	.145	.125	.317	1.300	3.302	.456	10.400	4.60	20	18 930	131	Fragmented
.057	.145	.125	.317	1.299	3.299	.456	10.392	5.16	23	21 230	146	Fragmented
.058	.147	.125	.317	1.298	3.297	.464	10.384	5.27	23	21 340	147	Fragmented
.058	.147	.125	.317	1.298	3.297	.464	10.384	4.82	21	19 510	135	Fragmented
.058	.147	.125	.317	1.298	3.297	.464	10.384	4.77	21	19 310	133	Fragmented
.116	.295	[a].249	.632	1.300	3.302	.466	5.225	10.73	48	20 790	143	Fragmented
.116	.295	[a].249	.632	1.301	3.304	.466	5.225	8.96	40	17 360	120	Fragmented
.116	.295	[a].249	.632	1.301	3.304	.466	5.225	9.28	41	17 990	124	Fragmented
.116	.295	[a].249	.632	1.301	3.304	.466	5.225	9.23	41	17 890	123	Fragmented
.116	.295	[b].249	.632	1.301	3.304	.466	5.225	7.52	33	14 570	100	Fragmented
.116	.295	[b].249	.632	1.301	3.304	.466	5.225	7.48	33	14 500	100	Fragmented
.116	.295	[b].249	.632	1.300	3.302	.466	5.221	7.30	32	14 150	98	Fragmented
.116	.295	[b].249	.632	1.301	3.304	.466	5.225	7.13	32	13 820	95	Fragmented
.117	.297	[a].249	.632	1.300	3.302	.470	5.221	10.04	45	19 270	133	Fragmented
.117	.297	[b].249	.632	1.300	3.302	.466	5.221	7.06	31	13 550	93	Fragmented
.174	.442	.378	.960	1.302	3.307	.460	3.444	10.20	45	12 600	87	Fragmented
.174	.442	.378	.960	1.303	3.310	.460	3.447	9.60	43	11 900	82	Fragmented
[c].174	.442	.378	.960	1.302	3.307	.460	3.444	16.90	75	20 900	144	Fragmented
[c].174	.442	.378	.960	1.302	3.307	.460	3.444	18.90	84	23 400	161	Fragmented
.175	.444	.378	.960	1.302	3.307	.463	3.444	9.16	41	11 300	78	Fragmented
.191	.485	.430	1.092	1.327	3.371	.444	3.086	7.90	35	8 670	60	Fragmented
.202	.513	.430	1.092	1.304	3.312	.470	3.033	9.80	44	10 300	71	Fragmented
.203	.516	.430	1.092	1.302	3.307	.472	3.028	9.60	43	10 000	69	Fragmented
.204	.518	.430	1.092	1.301	3.304	.475	3.026	11.00	49	11 000	76	Fragmented
.204	.518	.430	1.092	1.300	3.302	.475	3.023	10.60	47	11 000	76	Fragmented

[a]Oversized die shaft resulted in increased friction.

[b]Die with reworked die shaft.

[c]Not lubricated.

TABLE II.- SPECIMEN DIMENSIONS AND TEST RESULTS – Continued

t		r		D_i		t/r	D_i/r	$F_{f,av}$		$\sigma_{f,av}$		Operating regime
in.	cm	in.	cm	in.	cm			kips	kN	psi	MN/m^2	
2024-T3 aluminum alloy – continued												
0.232	0.589	0.506	1.285	1.303	3.310	0.458	2.575	13.80	61	12 300	85	Fragmented
.232	.589	.506	1.285	1.303	3.310	.458	2.575	13.90	62	12 400	85	Fragmented
[c].232	.589	.506	1.285	1.303	3.310	.458	2.575	20.80	93	18 600	128	Fragmented
[c].233	.592	.506	1.285	1.300	3.302	.460	2.569	21.00	93	18 700	129	Fragmented
.233	.592	.506	1.285	1.303	3.310	.460	2.575	11.30	50	10 100	70	Fragmented
.290	.737	.630	1.600	1.303	3.310	.460	2.068	15.40	68	10 600	73	Fragmented
.290	.737	.630	1.600	1.304	3.312	.460	2.070	15.20	68	10 500	72	Fragmented
.290	.737	.630	1.600	1.303	3.310	.460	2.606	14.20	63	9 800	68	Fragmented
.290	.737	.630	1.600	1.303	3.310	.460	2.606	15.00	67	10 300	71	Fragmented
.291	.739	.630	1.600	1.302	3.307	.462	2.067	15.20	68	10 400	72	Fragmented
[c].346	.879	.758	1.925	1.307	3.320	.456	1.724	28.70	128	16 000	110	Fragmented
.348	.884	.758	1.925	1.303	3.310	.459	1.719	18.40	82	10 200	70	Fragmented
.349	.886	.758	1.925	1.301	3.304	.460	1.716	17.60	78	9 800	68	Fragmented
[c].349	.886	.758	1.925	1.302	3.307	.460	1.718	34.80	155	19 200	132	Fragmented
[c].351	.892	.758	1.925	1.298	3.297	.463	1.712	24.00	107	13 200	91	Fragmented
.187	.475	.626	1.590	1.300	3.302	.299	2.077	5.10	23	5 840	40	Fragmented
.187	.475	.626	1.590	1.300	3.302	.299	2.077	4.57	20	5 230	36	Fragmented
.187	.475	.626	1.590	1.300	3.302	.299	2.077	4.80	21	5 500	38	Fragmented
.187	.475	.758	1.925	1.300	3.302	.247	1.715	4.22	19	4 830	33	Fragmented
.187	.475	.758	1.925	1.301	3.304	.247	1.716	4.00	18	4 570	32	Fragmented
.217	.551	.626	1.590	1.303	3.310	.347	2.081	7.00	31	6 750	47	Fragmented
.217	.551	.626	1.590	1.303	3.310	.348	2.081	6.80	30	6 530	45	Fragmented
.217	.551	.626	1.590	1.304	3.312	.348	2.083	6.90	31	6 630	46	Fragmented
.217	.551	.626	1.590	1.302	3.307	.347	2.080	7.10	32	6 860	47	Fragmented
.218	.554	.626	1.590	1.302	3.307	.348	2.080	7.10	32	6 820	47	Fragmented
.248	.630	.630	1.600	1.303	3.310	.394	2.068	9.14	41	7 560	52	Fragmented
.248	.630	.630	1.600	1.304	3.312	.394	2.070	9.82	44	8 120	56	Fragmented
.248	.630	.630	1.600	1.304	3.312	.394	2.070	8.90	40	7 360	51	Fragmented
.248	.630	.630	1.600	1.304	3.312	.394	2.070	9.90	44	8 180	56	Fragmented
.249	.632	.630	1.600	1.302	3.307	.395	2.067	9.75	43	8 040	55	Fragmented
.280	.711	.630	1.600	1.302	3.307	.444	2.067	11.90	53	8 540	59	Fragmented
.281	.714	.630	1.600	1.300	3.302	.446	2.063	11.60	52	8 310	57	Fragmented
.281	.714	.630	1.600	1.300	3.302	.446	2.063	12.40	55	8 880	61	Fragmented
.281	.714	.630	1.600	1.300	3.302	.446	2.063	12.30	55	8 820	61	Fragmented
.281	.714	.630	1.600	1.300	3.302	.446	2.063	12.30	55	8 820	61	Fragmented
.311	.790	.630	1.600	1.302	3.307	.494	2.067	16.90	75	10 700	74	Fragmented
.311	.790	.630	1.600	1.303	3.310	.494	2.068	16.00	71	10 200	70	Fragmented
.311	.790	.630	1.600	1.302	3.307	.494	2.067	16.60	74	10 500	72	Fragmented
.311	.790	.630	1.600	1.303	3.310	.494	2.068	17.00	76	10 800	74	Fragmented
.311	.790	.630	1.600	1.302	3.307	.494	2.067	17.30	77	11 000	76	Fragmented
.348	.884	.630	1.600	1.304	3.312	.552	2.070	32.10	143	17 800	123	Fragmented
.348	.884	.626	1.590	1.303	3.310	.556	2.081	32.80	146	18 200	125	Fragmented
.348	.884	.626	1.590	1.304	3.312	.556	2.083	32.60	145	18 100	125	Fragmented
.349	.886	.626	1.590	1.302	3.307	.558	2.080	32.20	143	17 800	123	Fragmented
.349	.886	.626	1.590	1.301	3.304	.558	2.078	34.90	155	19 300	133	Fragmented
.131	.333	.430	1.092	1.300	3.302	.305	3.023	4.65	21	7 900	54	Fragmented
.131	.333	.758	1.925	1.300	3.302	.172	1.715	4.23	19	7 900	54	Rolled
.132	.335	.430	1.092	1.299	3.299	.307	3.021	4.32	19	7 280	50	Fragmented
.132	.335	.430	1.092	1.300	3.302	.307	3.023	4.63	21	7 800	54	Fragmented
.132	.335	.430	1.092	1.299	3.299	.307	3.021	4.22	19	7 100	49	Fragmented
.132	.335	.430	1.092	1.299	3.299	.307	3.021	4.80	21	8 080	56	Fragmented

[c]Not lubricated.

TABLE II.- SPECIMEN DIMENSIONS AND TEST RESULTS – Continued

t		r		D_i		t/r	D_i/r	$F_{f,av}$		$\sigma_{f,av}$		Operating regime
in.	cm	in.	cm	in.	cm			kips	kN	psi	MN/m^2	
2024-T3 aluminum alloy – continued												
0.152	0.386	0.430	1.092	1.300	3.302	0.354	3.023	6.20	28	8 940	62	Fragmented
.152	.386	.430	1.092	1.300	3.302	.354	3.023	6.16	27	8 880	61	Fragmented
.152	.386	.430	1.092	1.303	3.310	.354	3.030	5.22	23	7 520	52	Fragmented
.153	.389	.758	1.925	1.300	3.302	.202	1.715	3.43	15	4 910	34	Rolled
.153	.389	.758	1.925	1.303	3.310	.202	1.719	3.51	16	5 020	35	Rolled
.173	.439	.430	1.092	1.304	3.312	.402	3.033	6.66	30	8 280	57	Fragmented
.174	.442	.430	1.092	1.302	3.307	.405	3.028	7.30	32	9 040	62	Fragmented
.174	.442	.430	1.092	1.302	3.307	.405	3.028	6.85	30	8 480	58	Fragmented
.174	.442	.430	1.092	1.302	3.307	.405	3.028	6.82	30	8 440	58	Fragmented
.174	.442	.430	1.092	1.302	3.307	.405	3.028	6.84	30	8 460	58	Fragmented
.196	.498	.430	1.092	1.301	3.304	.456	3.026	9.90	44	10 700	74	Fragmented
.196	.498	.430	1.092	1.302	3.307	.456	3.028	9.80	44	10 600	73	Fragmented
.196	.498	.430	1.092	1.302	3.307	.456	3.028	9.60	43	10 400	72	Fragmented
.196	.498	.430	1.092	1.301	3.304	.456	3.026	11.00	49	11 100	77	Fragmented
.197	.500	.430	1.092	1.300	3.302	.458	3.023	10.90	48	11 800	81	Fragmented
.218	.554	.430	1.092	1.301	3.304	.507	3.026	15.00	67	14 400	99	Fragmented
.218	.554	.430	1.092	1.302	3.307	.507	3.028	15.60	69	15 000	103	Fragmented
.239	.607	.430	1.092	1.303	3.310	.556	3.030	20.20	90	17 500	121	Fragmented
.239	.607	.430	1.092	1.303	3.310	.556	3.030	18.40	82	15 900	110	Fragmented
.240	.610	.430	1.092	1.301	3.304	.558	3.026	18.80	84	16 200	112	Fragmented
.240	.610	.430	1.092	1.301	3.304	.558	3.026	23.30	104	20 000	138	Fragmented
.240	.610	.430	1.092	1.302	3.307	.558	3.028	20.60	92	17 700	122	Fragmented
.240	.610	.430	1.092	1.302	3.307	.558	3.028	21.70	97	18 700	129	Fragmented
.261	.663	.430	1.092	1.302	3.307	.607	3.028	28.40	126	22 100	152	Fragmented
.261	.663	.430	1.092	1.302	3.307	.607	3.028					Buckled
.261	.663	.430	1.092	1.302	3.307	.607	3.028					Buckled
.261	.663	.430	1.092	1.302	3.307	.607	3.028					Buckled
.261	.663	.430	1.092	1.302	3.307	.607	3.028					Buckled
.057	.145	[b].249	.632	1.299	3.299	.229	5.217	2.67	11	10 990	76	Rolled
.057	.145	[b].249	.632	1.300	3.302	.229	5.221	2.81	12	11 560	80	Rolled
.058	.147	[b].249	.632	1.298	3.296	.233	5.213	2.91	12	11 980	83	Rolled
.058	.147	[b].249	.632	1.298	3.296	.233	5.213	2.73	12	11 230	77	Rolled
.074	.188	[b].249	.632	1.300	3.302	.297	5.221	3.26	15	10 220	70	Fragmented
.074	.188	[b].249	.632	1.300	3.302	.297	5.221	2.74	12	8 590	59	Fragmented
.075	.191	[b].249	.632	1.299	3.299	.301	5.217	2.78	12	8 580	59	Fragmented
.087	.221	[b].249	.632	1.299	3.299	.349	5.217	3.39	15	8 940	62	Fragmented
.087	.221	[b].249	.632	1.299	3.299	.349	5.217	3.48	15	9 180	63	Fragmented
.087	.221	[b].249	.632	1.299	3.299	.349	5.217	3.65	16	9 630	66	Fragmented
.099	.251	[b].249	.632	1.301	3.304	.398	5.217	4.54	20	10 440	72	Fragmented
.099	.251	[b].249	.632	1.301	3.304	.398	5.217	4.18	19	9 610	66	Fragmented
.099	.251	[b].249	.632	1.301	3.304	.398	5.217	4.56	16	10 480	72	Fragmented
.112	.284	[b].249	.632	1.300	3.302	.450	5.221	6.70	30	13 480	93	Fragmented
.112	.284	[b].249	.632	1.300	3.302	.450	5.221	6.57	29	13 220	91	Fragmented
.112	.284	[b].249	.632	1.300	3.302	.450	5.221	6.39	28	12 860	89	Fragmented
.112	.284	[b].249	.632	1.300	3.302	.450	5.221	6.71	30	13 500	93	Fragmented
.112	.284	[b].249	.632	1.301	3.304	.450	5.221	6.74	30	13 560	93	Fragmented
.125	.318	[b].249	.632	1.301	3.304	.502	5.221	9.37	42	16 730	115	Fragmented
.125	.318	[b].249	.632	1.300	3.302	.502	5.221	9.60	43	17 140	118	Fragmented
.125	.318	[b].249	.632	1.300	3.302	.502	5.221	9.71	43	17 340	120	Fragmented
.132	.335	[b].249	.632	1.296	3.292	.530	5.221	10.61	47	17 890	123	Fragmented
.132	.335	[b].249	.632	1.299	3.299	.530	5.221	10.26	46	17 300	119	Fragmented
.132	.335	[b].249	.632	1.300	3.302	.530	5.221	11.65	52	19 650	135	Fragmented
.132	.335	[b].249	.632	1.299	3.299	.530	5.217	10.89	48	18 360	127	Fragmented

[b]Die with reworked die shaft.

TABLE II.- SPECIMEN DIMENSIONS AND TEST RESULTS – Continued

t		r		D_i		t/r	D_i/r	$F_{f,av}$		$\sigma_{f,av}$		Operating regime
in.	cm	in.	cm	in.	cm			kips	kN	psi	MN/m^2	
2024-T3 aluminum alloy – concluded												
0.138	0.351	[b]0.249	0.632	1.299	3.299	0.554	5.217	13.65	61	21 880	151	Fragmented
.138	.351	[b].249	.632	1.299	3.299	.554	5.217	12.22	54	19 610	135	Fragmented
.138	.351	[b].249	.632	1.299	3.299	.554	5.217	11.64	52	18 680	129	Fragmented
.150	.381	[b].249	.632	1.300	3.302	.600	5.221	21.86	97	32 010	221	Fragmented
.150	.381	[b].249	.632	1.300	3.302	.600	5.221	20.65	92	30 230	208	Fragmented
.150	.381	[b].249	.632	1.300	3.302	.600	5.221	22.32	99	32 680	225	Fragmented
.150	.381	[b].249	.632	1.300	3.302	.600	5.221	19.09	85	27 960	193	Fragmented
.152	.386	[b].249	.632	1.300	3.302	.610	5.221	27.79	124	40 100	276	Fragmented
.152	.386	[b].249	.632	1.303	3.310	.610	5.221	25.24	112	36 320	250	Fragmented
.152	.386	[b].249	.632	1.300	3.302	.610	5.221	22.60	101	32 610	225	Fragmented
.153	.389	[b].249	.632	1.300	3.302	.614	5.221	24.36	108	34 900	241	Fragmented
.218	.554	.738	1.875	3.103	7.882	.295	4.205	16.01	71	7 040	49	Oversized die shaft
.218	.554	.738	1.875	3.103	7.882	.295	4.205	17.17	76	7 550	52	Fragmented
.219	.556	.738	1.875	3.101	7.877	.297	4.202					Buckled
.254	.645	.738	1.875	3.102	7.879	.344	4.203					Buckled
.254	.645	.738	1.875	3.104	7.884	.344	4.206	27.45	122	10 240	71	Fragmented
.259	.658	.738	1.875	3.108	7.894	.351	4.211	20.07	89	7 326	51	Fragmented
.290	.737	.738	1.875	3.105	7.887	.393	4.207	21.80	97	7 050	49	Fragmented
.292	.742	.738	1.875	3.118	7.920	.391	4.225	27.01	120	8 640	60	Fragmented
.327	.831	.738	1.875	3.114	7.910	.443	4.220	39.11	174	11 060	76	Fragmented
.327	.831	.738	1.875	3.112	7.904	.443	4.217	34.91	155	9 880	68	Fragmented
.328	.833	.738	1.875	3.102	7.879	.444	4.203	31.27	139	8 850	61	Fragmented
.332	.843	.738	1.875	3.105	7.887	.450	4.207	35.60	158	9 930	68	Fragmented
.364	.925	.738	1.875	3.112	7.904	.493	4.217	52.03	231	13 090	90	Fragmented
.364	.925	.738	1.875	3.112	7.904	.493	4.217	54.34	242	13 670	94	Fragmented
.365	.927	.738	1.875	3.104	7.884	.495	4.206					Broke die
.365	.927	.738	1.875	3.112	7.904	.495	4.217	54.92	244	13 770	95	Fragmented
.400	1.016	.738	1.875	3.116	7.915	.542	4.222	74.73	332	16 910	117	Fragmented
.400	1.016	.738	1.875	3.114	7.910	.542	4.220	74.24	330	16 810	116	Fragmented
.404	1.026	.738	1.875	3.097	7.866	.547	4.196	75.66	337	17 030	117	Fragmented
.405	1.029	.738	1.875	3.112	7.904	.549	4.217	77.58	345	17 340	120	Fragmented
.410	1.041	.738	1.875	3.110	7.899	.556	4.214	74.79	333	16 490	114	Fragmented
.414	1.052	.738	1.875	3.109	7.897	.561	4.213	78.04	347	17 030	117	Fragmented
.429	1.090	.738	1.875	3.107	7.892	.581	4.210					Buckled
.430	1.092	.738	1.875	3.107	7.892	.583	4.210					Buckled
Chrome-molybdenum steel (AISI 4130) in a cold-water-quenched condition												
0.065	0.165	0.195	0.495	0.870	2.210	0.333	4.462	6.60	29	34 700	239	Fragmented
.065	.165	.195	.495	.870	2.210	.333	4.462	7.33	33	38 400	264	Fragmented
.065	.165	.158	.401	.870	2.210	.411	5.506	12.10	54	63 400	437	Fragmented
.065	.165	.164	.417	.870	2.210	.396	5.305	9.14	41	47 800	330	Fragmented
.065	.165	.101	.257	.870	2.210	.644	8.614	24.90	111	130 400	899	Fragmented
.065	.165	.101	.257	.870	2.210	.644	8.614	24.00	107	126 000	869	Fragmented
.065	.165	.101	.257	.870	2.210	.644	8.614	24.30	108	127 000	876	Fragmented

[b]Die with reworked die shaft.

TABLE II.- SPECIMEN DIMENSIONS AND TEST RESULTS – Concluded

t		r		D_i		t/r	D_i/r	$F_{f,av}$		$\sigma_{f,av}$		Operating regime
in.	cm	in.	cm	in.	cm			kips	kN	psi	MN/m^2	
AZ31B magnesium alloy												
0.065	0.165	0.101	0.257	0.870	2.210	0.644	8.614					Buckled
.065	.165	.115	.292	.870	2.210	.644	7.565					Buckled
.065	.165	.125	.317	.870	2.210	.520	6.960	1.97	9	10 300	71	Fragmented
.065	.165	.125	.317	.870	2.210	.520	6.960	2.00	9	10 500	72	Fragmented
.065	.165	.125	.317	.870	2.210	.520	6.960					Fragmented then buckled
.065	.165	.132	.335	.870	2.210	.492	6.591	1.79	8	9 360	65	Fragmented
.065	.165	.132	.335	.870	2.210	.492	6.591	1.84	8	9 640	66	Fragmented
.065	.165	.132	.335	.870	2.210	.490	6.591	1.92	9	10 100	70	Fragmented
.065	.165	.164	.417	.870	2.210	.396	5.305	1.39	6	7 280	50	Fragmented
.065	.165	.164	.417	.870	2.210	.396	5.305	1.30	6	6 810	47	Fragmented
.065	.165	.164	.417	.870	2.210	.396	5.305	1.25	6	6 540	45	Fragmented
.065	.165	.155	.394	.870	2.210	.419	5.613	1.57	7	8 220	57	Fragmented
.065	.165	.155	.394	.870	2.210	.419	5.613	1.57	7	8 220	57	Fragmented
.065	.165	.158	.401	.870	2.210	.411	5.506	1.50	7	7 860	54	Fragmented
.065	.165	.158	.401	.870	2.210	.411	5.506	1.76	8	9 220	64	Fragmented
.065	.165	.158	.401	.870	2.210	.411	5.506	1.66	7	8 700	60	Fragmented
.065	.165	.195	.495	.870	2.210	.333	4.462	1.27	6	6 650	46	Fragmented
.065	.165	.195	.495	.870	2.210	.333	4.462	1.34	6	7 000	48	Fragmented
.065	.165	.195	.495	.870	2.210	.333	4.462	1.31	6	6 860	47	Fragmented
7075-T6 aluminum alloy												
0.065	0.165	0.195	0.495	0.870	2.210	0.333	4.461	1.47	7	7 720	53	Fragmented
.065	.165	.195	.495	.870	2.210	.333	4.461	1.37	6	7 170	49	Fragmented
.065	.165	.195	.495	.870	2.210	.333	4.461	1.34	6	7 140	49	Fragmented
.065	.165	.158	.401	.870	2.210	.411	5.506	1.94	9	10 200	70	Fragmented
.065	.165	.158	.401	.870	2.210	.411	5.506	2.01	9	10 500	72	Fragmented
.065	.165	.158	.401	.870	2.210	.411	5.506	1.88	8	9 880	68	Fragmented
.065	.165	.155	.394	.870	2.210	.419	5.613	2.07	9	10 800	74	Fragmented
.065	.165	.155	.394	.870	2.210	.419	5.613	1.99	9	10 400	72	Fragmented
.065	.165	.155	.394	.870	2.210	.419	5.613	1.92	9	10 100	70	Fragmented
.065	.165	.164	.417	.870	2.210	.396	5.305	1.62	7	8 500	59	Fragmented
.065	.165	.164	.417	.870	2.210	.396	5.305	1.81	8	9 480	65	Fragmented
.065	.165	.164	.417	.870	2.210	.396	5.305	1.62	7	8 480	58	Fragmented
.065	.165	.132	.335	.870	2.210	.492	6.591	2.79	12	14 600	101	Fragmented
.065	.165	.132	.335	.870	2.210	.492	6.591	2.83	13	14 800	102	Fragmented
.065	.165	.132	.335	.870	2.210	.492	6.591	2.78	12	14 600	101	Fragmented
.065	.165	.125	.318	.870	2.210	.520	6.960	3.41	15	17 900	123	Fragmented
.065	.165	.125	.318	.870	2.210	.520	6.960	3.84	17	20 100	139	Fragmented
.065	.165	.125	.318	.870	2.210	.520	6.960	3.65	16	19 100	132	Fragmented
.065	.165	.115	.292	.870	2.210	.565	7.565	4.37	19	22 900	158	Fragmented
.065	.165	.115	.292	.870	2.210	.565	7.565	4.25	19	22 300	154	Fragmented
.065	.165	.115	.292	.870	2.210	.565	7.565	4.11	18	21 500	148	Fragmented
.065	.165	.101	.257	.870	2.210	.644	8.614	7.66	34	40 100	276	Fragmented
.065	.165	.101	.257	.870	2.210	.644	8.614	6.94	31	36 300	250	Fragmented
.065	.165	.101	.257	.870	2.210	.644	8.614	7.38	33	38 700	267	Fragmented

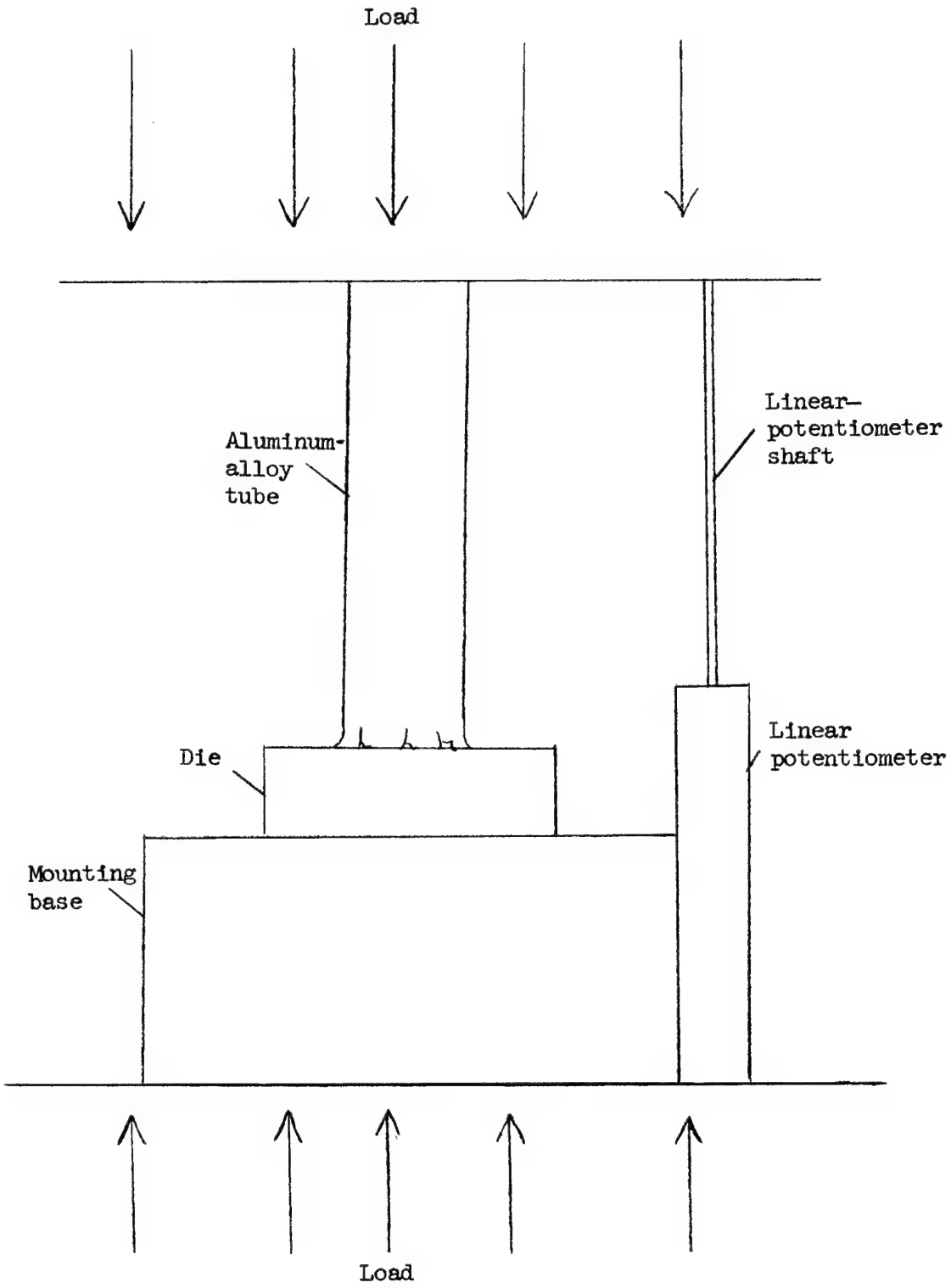

Figure 1.- Sketch of test setup.

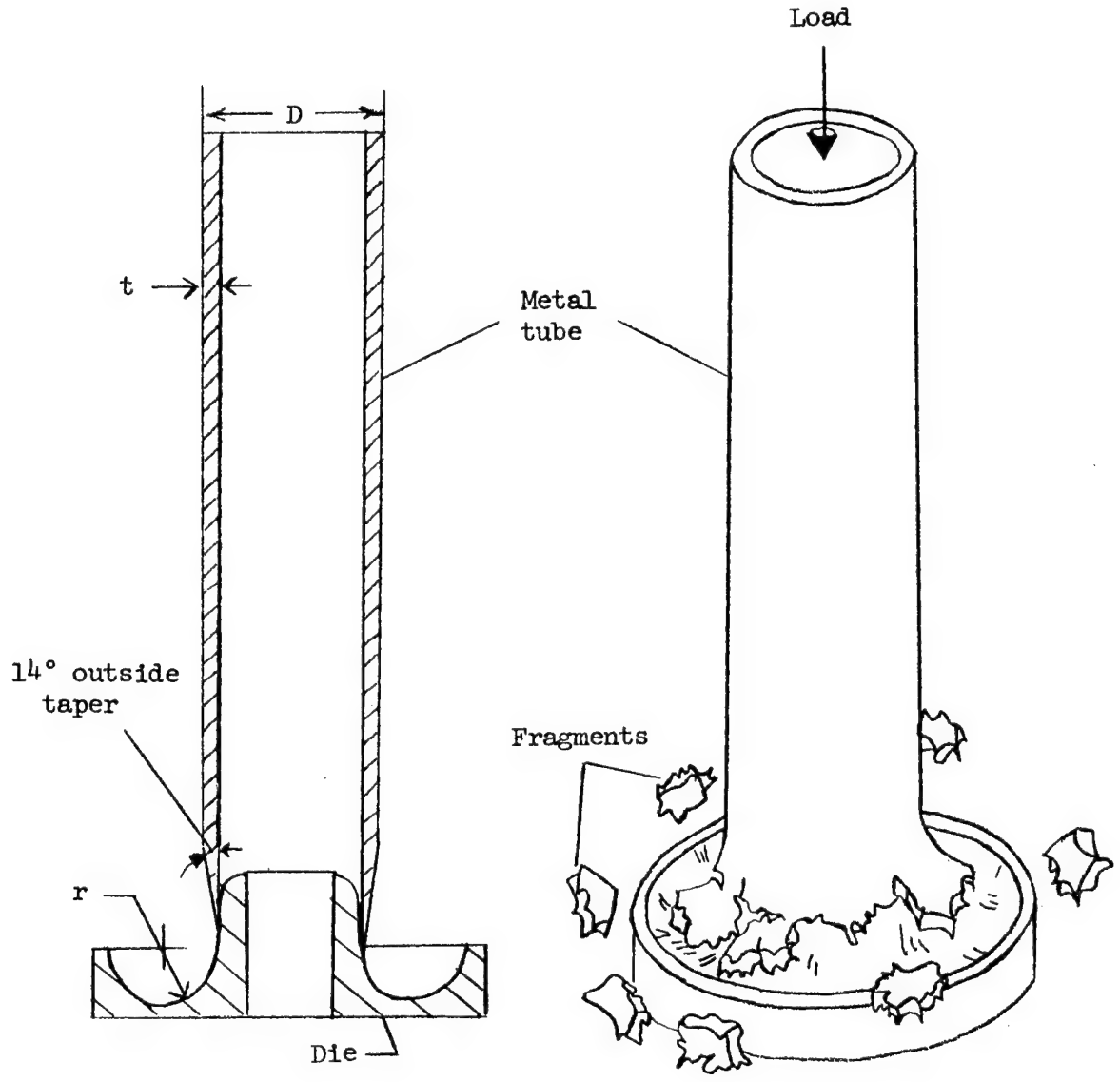

Figure 2.- Sketch illustrating fragmenting process.

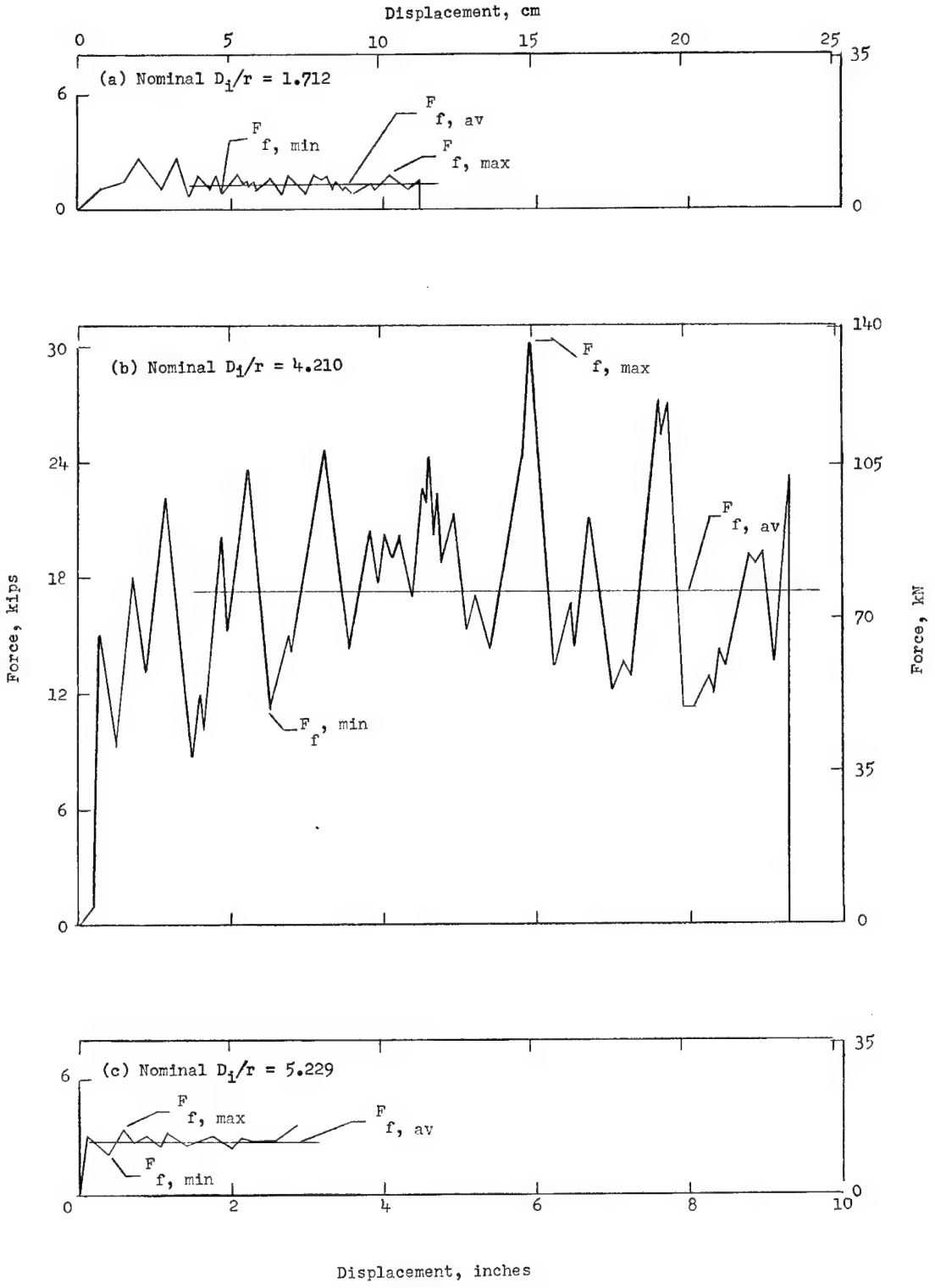

Figure 3.- Typical axial-force variations with displacement for 2024-T3 aluminum alloy. Nominal $t/r = 0.300$.

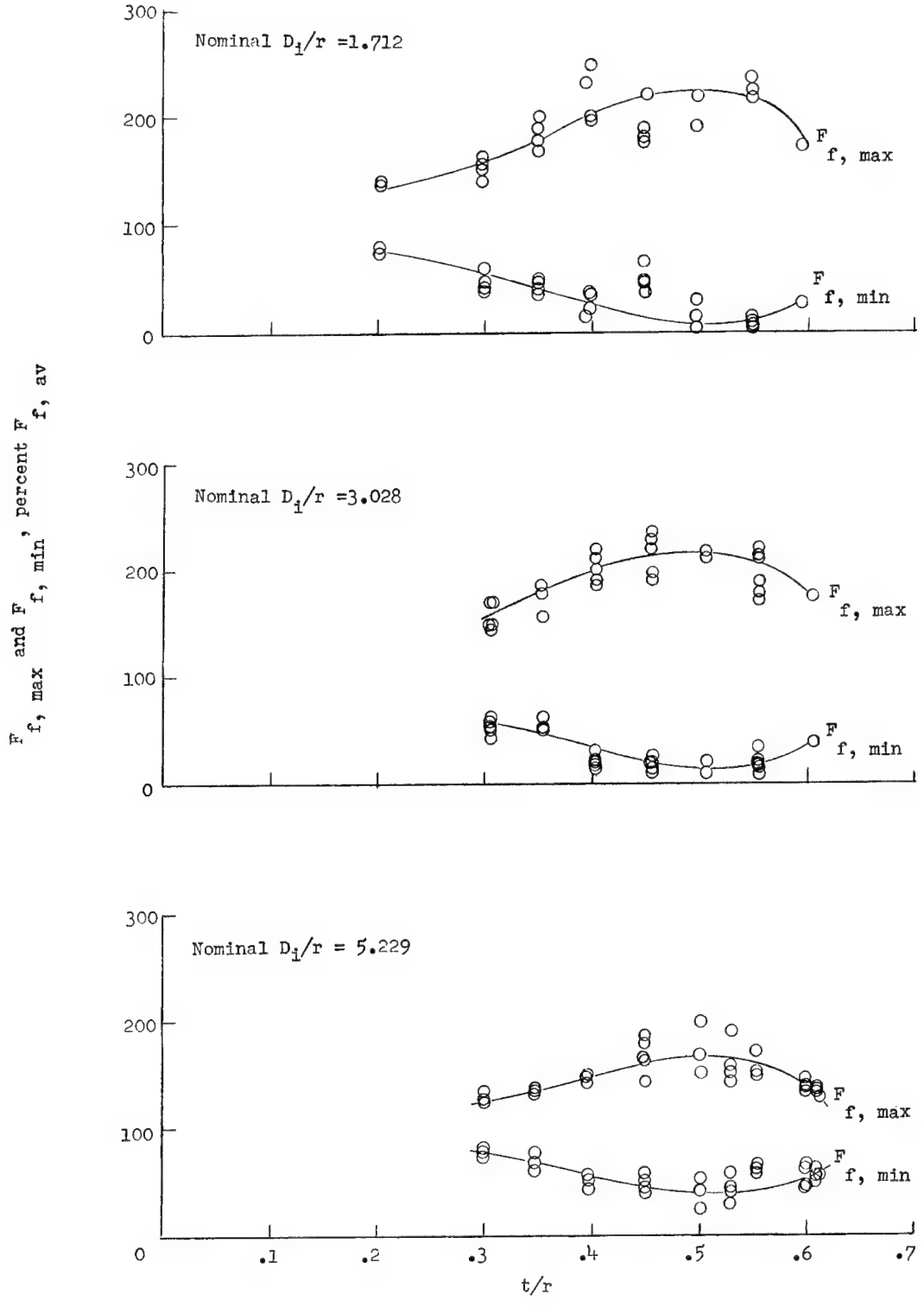

Figure 4.- Variation of maximum and minimum fragmenting force fluctuations with tube-wall-thickness—die-radius ratio for 2024-T3 aluminum alloy.

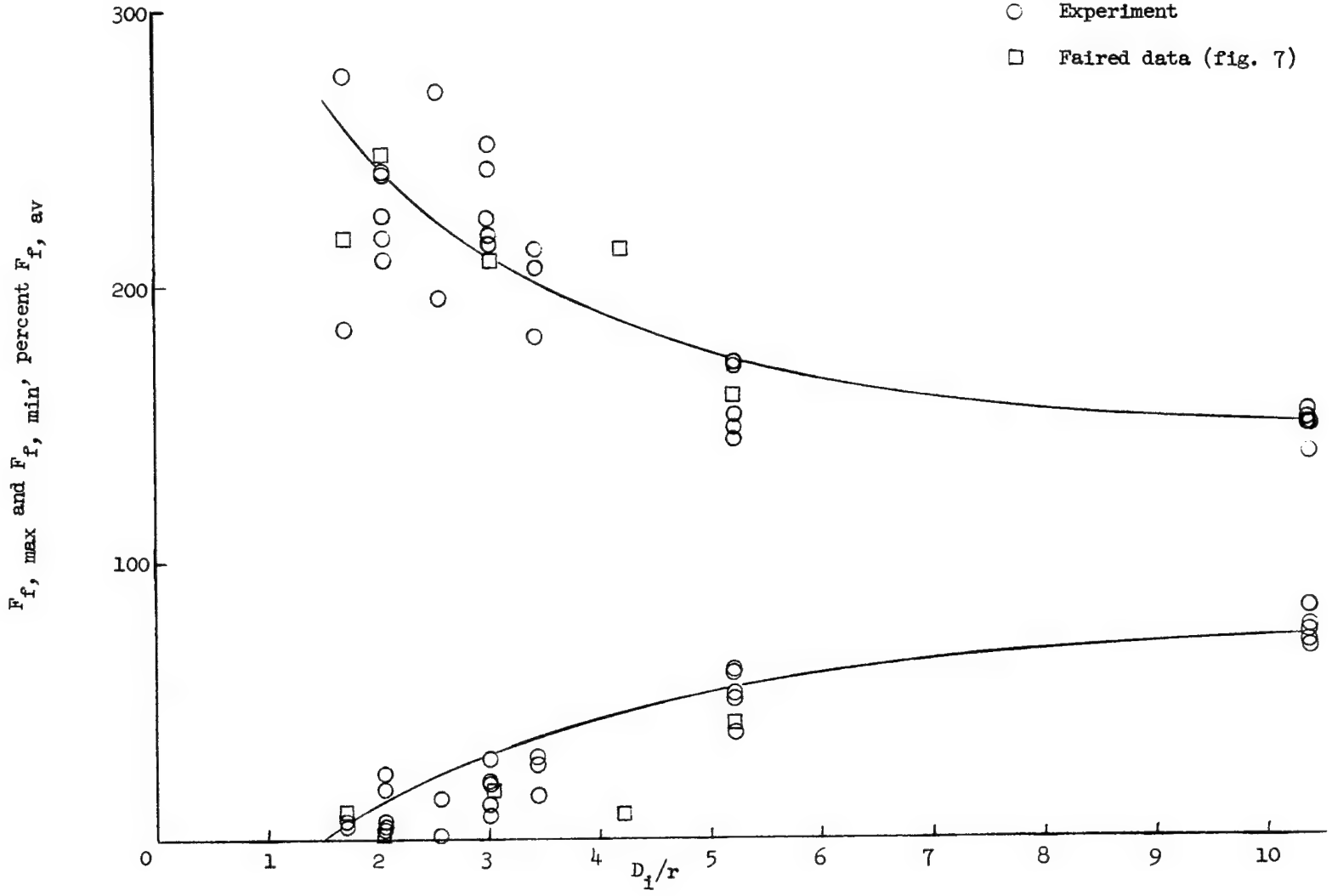

Figure 5.- Variation of maximum and minimum fragmenting force fluctuations with tube-inside-diameter—die-radius ratio for 2024-T3 aluminum alloy. Nominal t/r = 0.460.

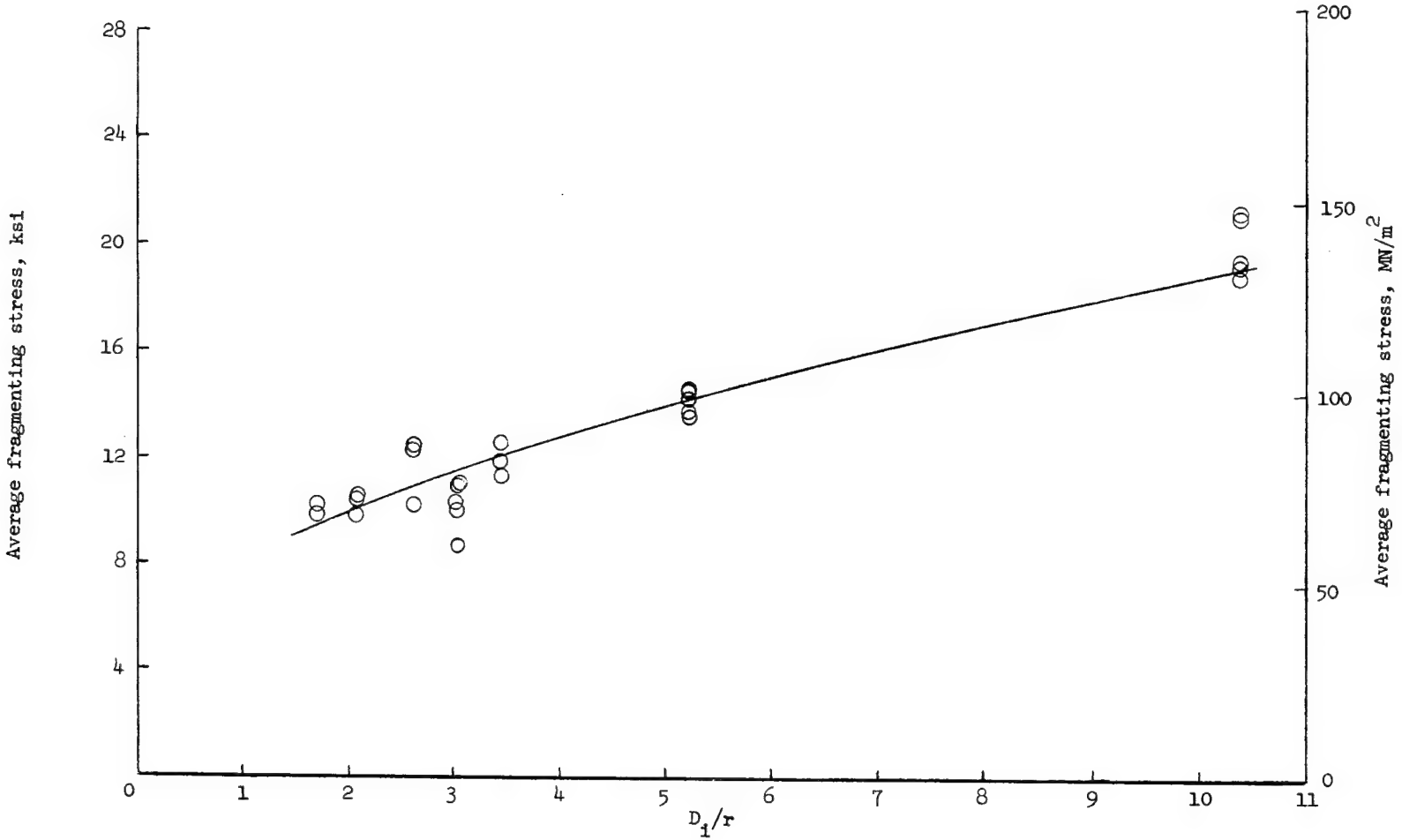

Figure 6.- Variation of average fragmenting stress with tube-inside-diameter—die-radius ratio for 2024-T3 aluminum alloy. Nominal $t/r = 0.460$.

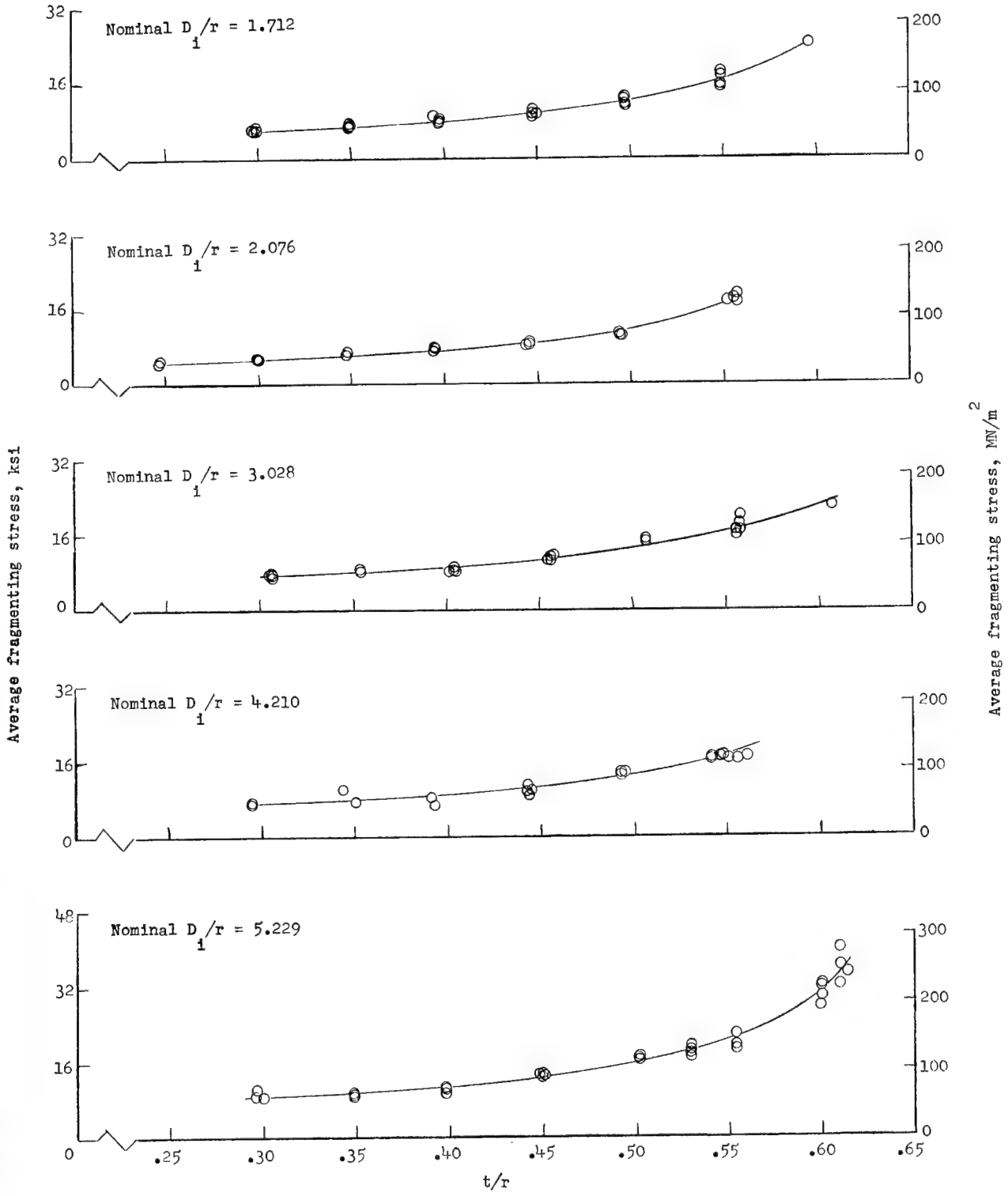

Figure 7.- Variation of average fragmenting stress with tube-wall-thickness—die-radius ratio for 2024-T3 aluminum alloy.

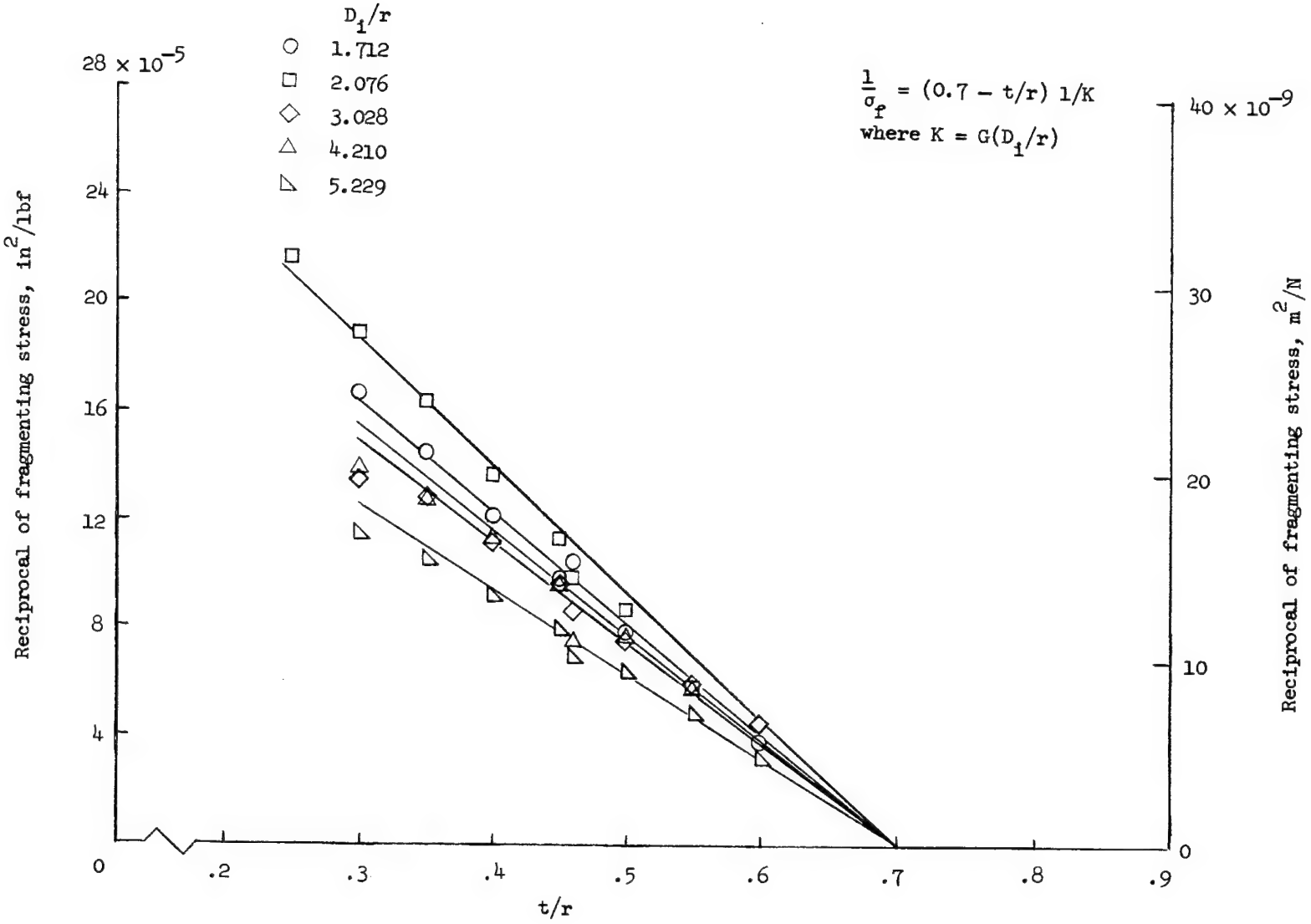

Figure 8.- Reciprocal of the average fragmenting stress as a function of tube-wall-thickness—die-radius ratio for 2024-T3 aluminum alloy.

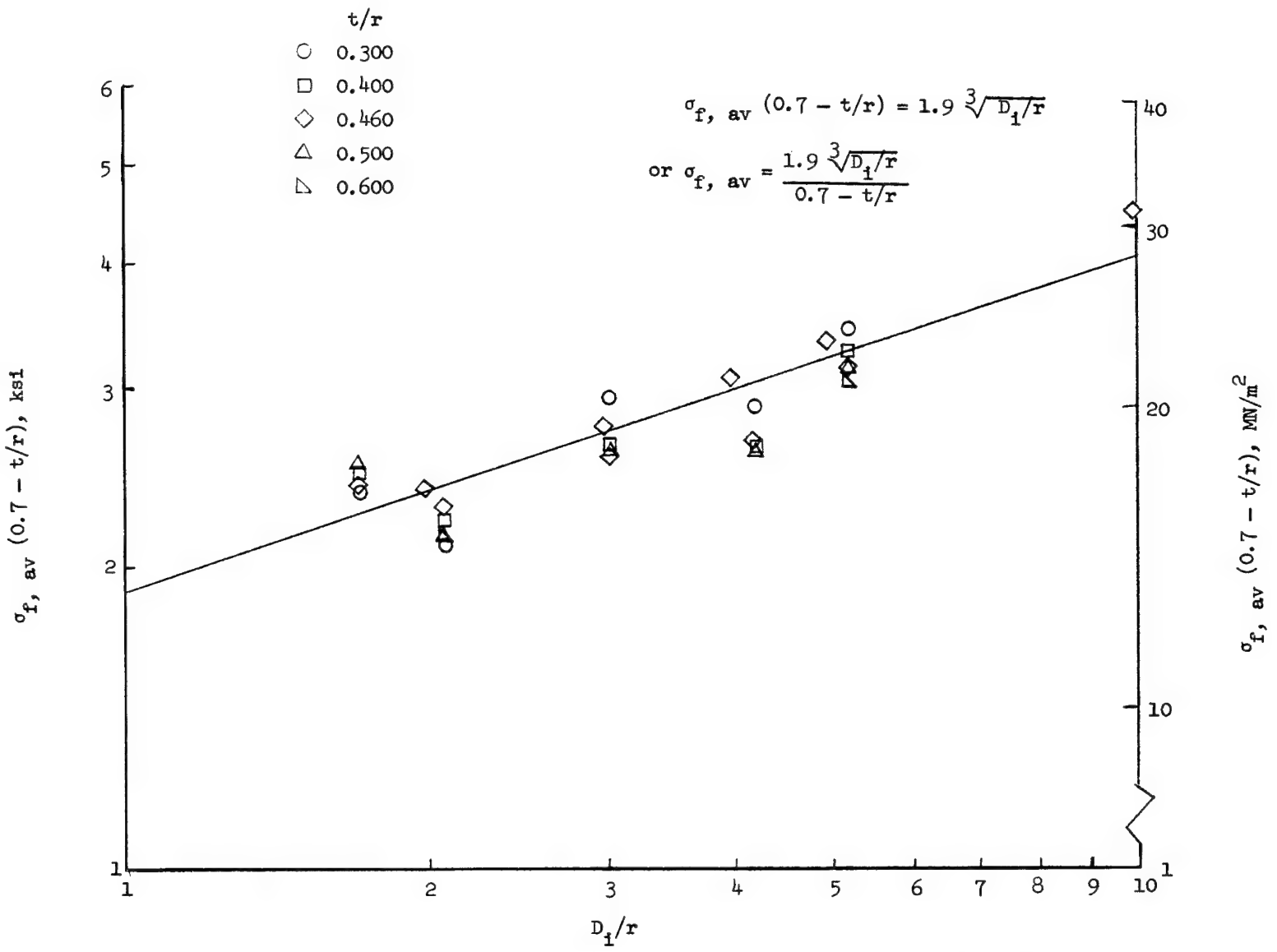

Figure 9.- Variation of product of average fragmenting stress and function of tube-wall-thickness—die-radius ratio with tube-inside-diameter—die-radius ratio for 2024-T3 aluminum alloy.

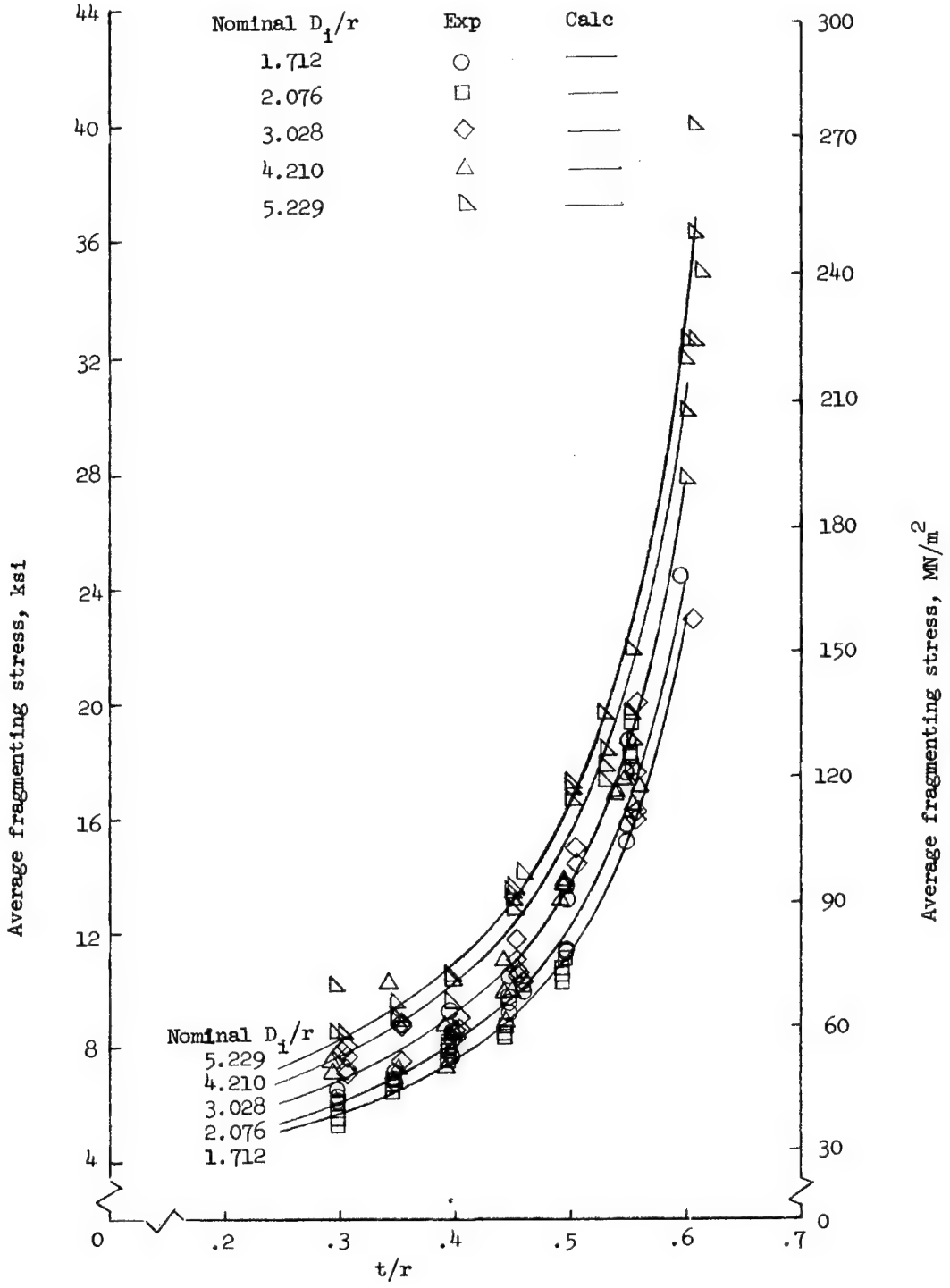

(a) Comparison of experimental and computed data.

Figure 10.- Variation of average fragmenting stress with the principal parameters for 2024-T3 aluminum alloy.

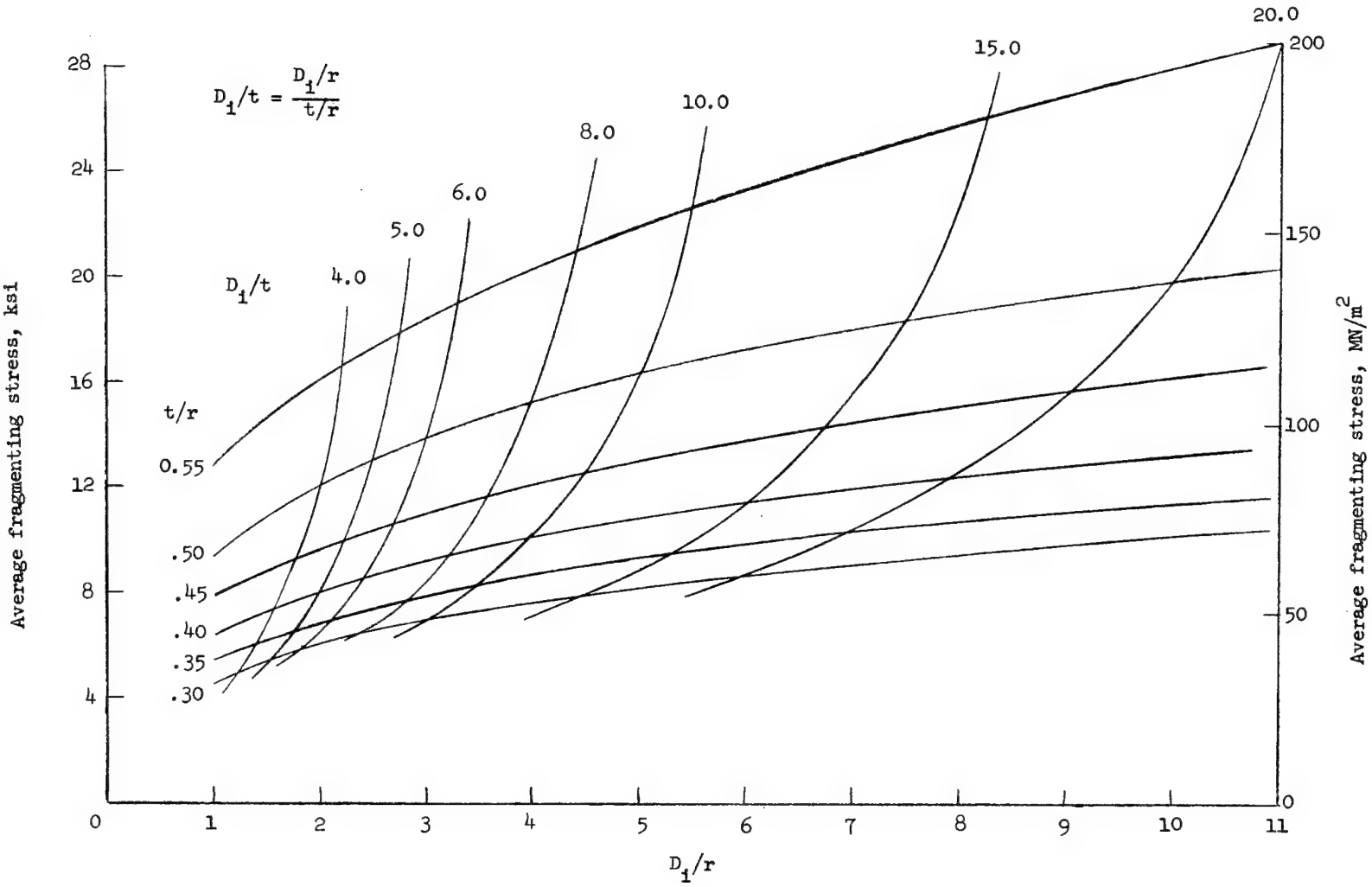

(b) Design chart.

Figure 10.- Concluded.

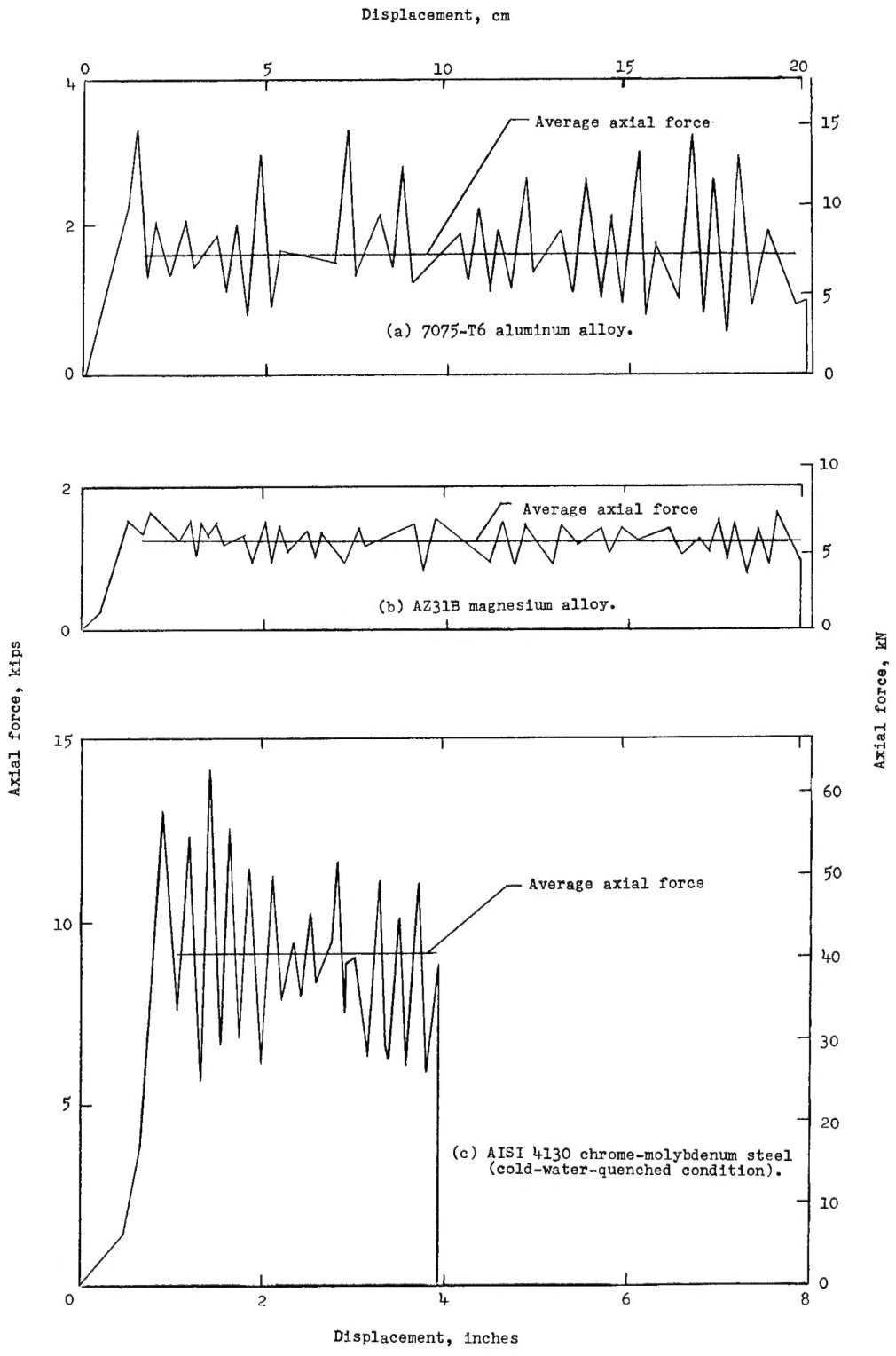

Figure 11.- Typical axial-force variations with displacement for various materials. Nominal t/r = 0.396.

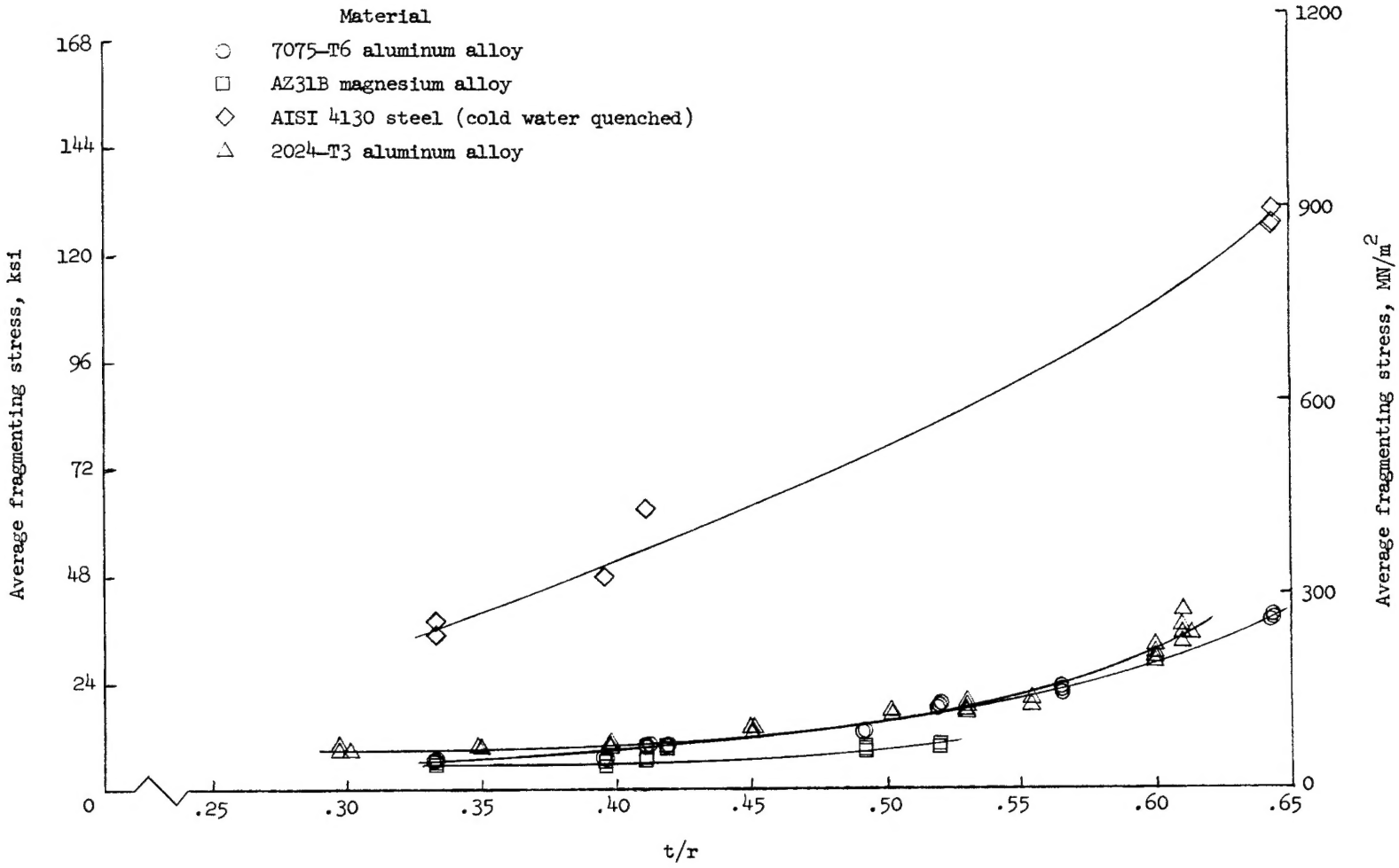

Figure 12.- Variation of average fragmenting stress with tube-wall-thickness—die-radius ratio for four materials. Range of D_i/r from 4.461 to 8.614.

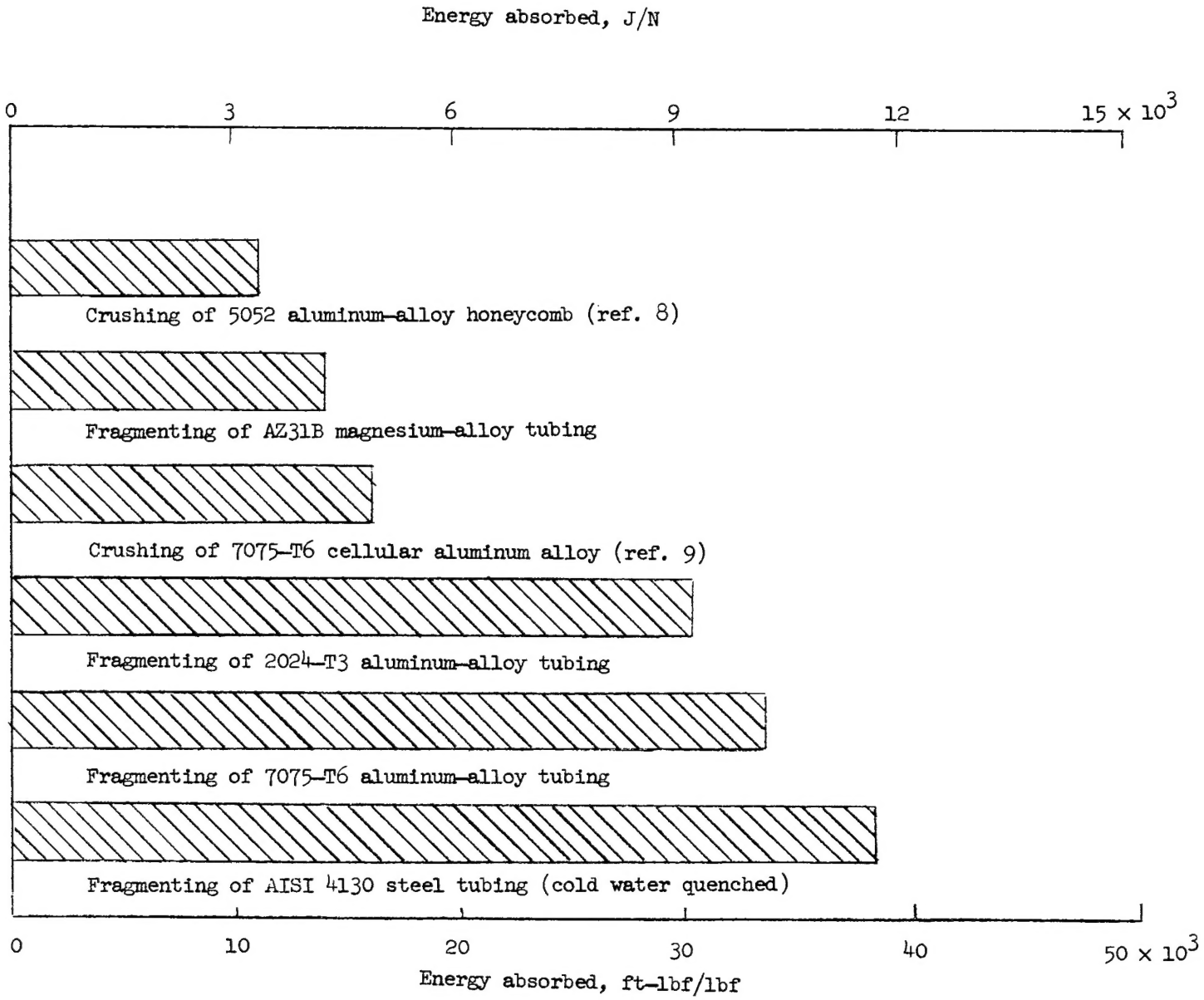

Figure 13.- Energy-absorption capabilities of various materials and processes.

"The aeronautical and space activities of the United States shall be conducted so as to contribute . . . to the expansion of human knowledge of phenomena in the atmosphere and space. The Administration shall provide for the widest practicable and appropriate dissemination of information concerning its activities and the results thereof."

—NATIONAL AERONAUTICS AND SPACE ACT OF 1958

NASA SCIENTIFIC AND TECHNICAL PUBLICATIONS

TECHNICAL REPORTS: Scientific and technical information considered important, complete, and a lasting contribution to existing knowledge.

TECHNICAL NOTES: Information less broad in scope but nevertheless of importance as a contribution to existing knowledge.

TECHNICAL MEMORANDUMS: Information receiving limited distribution because of preliminary data, security classification, or other reasons.

CONTRACTOR REPORTS: Technical information generated in connection with a NASA contract or grant and released under NASA auspices.

TECHNICAL TRANSLATIONS: Information published in a foreign language considered to merit NASA distribution in English.

TECHNICAL REPRINTS: Information derived from NASA activities and initially published in the form of journal articles.

SPECIAL PUBLICATIONS: Information derived from or of value to NASA activities but not necessarily reporting the results of individual NASA-programmed scientific efforts. Publications include conference proceedings, monographs, data compilations, handbooks, sourcebooks, and special bibliographies.

Details on the availability of these publications may be obtained from:

SCIENTIFIC AND TECHNICAL INFORMATION DIVISION

NATIONAL AERONAUTICS AND SPACE ADMINISTRATION

Washington, D.C. 20546